EUROPEAN ORGANIZATION FOR NUCLEAR RESEARCH

ELASTIC SCATTERING OF NEGATIVE KAONS ON POLARIZED PROTONS BETWEEN 1.4 AND 2.4 GeV/c

C. Daum, F. Erné[*)], J.P. Lagnaux[**)], J.C. Sens[*)], M. Steuer[***)] and F. Udo[*)]

CERN, Geneva, Switzerland

ABSTRACT

The elastic scattering of negative kaons on polarized protons has been investigated in the range of kaon momenta: 1.4-2.4 GeV/c. Measurements of intensity and polarization angular distributions are presented for 19 incident momenta in this range. The results are parametrized in Legendre expansion coefficients. The possibility of extracting resonance parameters from the data is discussed.

Geneva - 8 April 1968

(Submitted to Nuclear Physics)

---

*) Visitor from the Foundation for Fundamental Research of Matter (FOM), the Netherlands.

**) Visitor from Institut Interuniversitaire des Sciences nucléaires, Bruxelles.

***) Visitor from the Institute for High-Energy Physics of the Austrian Academy of Sciences, Vienna.

1. INTRODUCTION

This paper gives an account of measurements of the angular distributions of polarization and differential cross-section in the elastic scattering of negative kaons on polarized protons at incident laboratory momenta between 1.4 and 2.4 GeV/c. Available data on differential cross-sections[1] in this range of momenta show that the elastic scattering is dominated by diffraction phenomena and hence that resonances such as have been revealed by total cross-section data[2] will only manifest themselves as small perturbances on a large background.

The present experiment explores the elastic channel in detail by providing polarization and differential cross-section data at narrow (50 MeV/c) incident momentum intervals and over a large interval in scattering angle (typically from +0.9 to -0.8 in $\cos \vartheta_{c.m.}$).

Section 2 describes the experiment; Section 3 presents the procedure followed in the reduction of the data. Section 4 presents the results and a discussion of the data.

Preliminary results of this experiment have been reported previously[3].

2. DESCRIPTION OF THE EXPERIMENT

2.1 Features of the design

The experiment has been performed by detecting elastically scattered particles in counter hodoscopes placed around a target containing vertically polarized protons in a separated kaon beam of the CERN Proton Synchrotron. The events were identified by determining the polar and azimuthal angles of the two charged secondaries in elements of counter hodoscopes to the left and to the right of the beam axis, without further identifying the nature of the particle. This was realized in two stages: first, by electronically requiring a coincidence between one and only one particle in the left hodoscopes, and one and only one particle in the right hodoscopes; second, by imposing on these events the condition of coplanarity in off-line computer analysis. This arrangement enabled us to use the non-coplanar events to determine the background among the coplanar events.

The fact that the nature of the emerging particles is not identified gives rise to the possibility of confusion between elastic events and "reverse-elastic" events, in which the kaon and the recoil proton are interchanged. Section 3 describes to which extent this effect influences the results.

2.2 Beam

The data have been taken in a secondary beam, the m_{4b} beam[4], derived from internal target No. 1 of the CERN PS. The beam is 37 m long, and contains an electrostatic separator of 9 m length with an electric field of 45-50 kV/cm, to reject pions and antiprotons from the beam. The rejection factor obtained at a given beam momentum depends on the conditions of focusing and acceptance to which the beam is tuned; in the conditions of the experiment, the separator reduced the π/K ratio from 250 to 10 at 1.4 GeV/c; at 2.0 GeV/c the reduction was from 200 to 80; above 2 GeV/c the separation deteriorates rapidly.

The beam has been focused on the polarized target 2.5 m behind the exit of the last magnet in the beam. At this point the measured angular divergence was typically $\pm 1°$ in the horizontal plane and $\pm 0.3°$ in the vertical plane. The dispersion of the beam and the multiple scattering in the beam counters produced a beam spot of typically 7 mm vertical and 10 mm horizontal; between 55% and 75% of the incident particles were actually focused on the target.

2.3 Polarized target

The polarized target was of the LMN type $(La_2Mg_3(NO_3)_{12} \cdot 24H_2O)$. It consisted of two crystals together forming a rectangular block of 12 × 12 × 45 mm. Construction and performance of the target are described elsewhere[5].

The experiment could be done in a fixed geometry, because the polarization is reversed simply by shifting the microwave frequency dissipated in the crystal, keeping the direction of the magnetic field constant. The density of free polarizable protons in the LMN material is 0.067 g/cm^3 to be compared to the total density of the material of 2.0 g/cm^3. The mean free path for elastic scattering of kaons on free protons in this target is 4400 cm, while for elastic scattering on bound protons it is

820 cm. One thus expects about five times as many elastic scatters on bound as on free protons. The total momentum loss of the beam in the 45 mm long target was 34 MeV/c throughout the range of incident momenta in this experiment. The target is placed in a vertical magnetic field of 18.5 kG produced by a magnet with polefaces of 12 cm diameter and a gap of 7 cm. The magnet has an open structure allowing free access along 300° in the horizontal plane and ±15° in azimuth.

A dummy target, of the same specific weight, average atomic weight and charge as the polarized target, but without free protons, has been used to check the background spectra. The target polarization was typically 0.65 during the measurements. The absolute error in the calibration of the polarization is 0.03 (see Ref. 5).

2.4 Arrangement of counters

Figure 1 shows the assembly of counters, the target, the magnet, and the cryostat. The incident beam has been defined by scintillators B_1 and B_2. The counters C_1 and C_2 are two, ethylene-filled, threshold gas Čerenkov counters of 46 cm effective length and 11 cm diameter. They tag unwanted particles which were not removed by the separator. Counter C_2 was permanently installed and set at about 25 atm to count pions, muons, and electrons. Counter C_1 was rolled into the beam for the data taken at 2.2 GeV/c and above, and was set at 42 atm; it then counted pions, muons, electrons, and kaons, so that a $C_1 \bar{C}_2$ signal distinguished kaons also against antiprotons which were poorly rejected by the separator at these momenta. As multiple scattering in C_1 seriously affected the beam spot, this counter was only rolled into the beam when the amount of antiprotons in the beam was more than 1% of the number of incident kaons. The rejection efficiencies of C_1 and C_2 were greater than 99.98%. In this way both the pion and antiproton contamination in the accepted kaon beam was kept below 1% at all incident momenta.

Counter B_3 was a 15 mm diameter, 2 mm thick scintillator placed close to the target, in order to count the focused kaon rate. It contained 0.02 g/cm^2 free protons, versus 0.3 g/cm^2 in the target. Hence this counter had to be shielded from the hodoscopes by an anticounter (B_4), shaped as a shield with a hole in the centre. An anticounter B_5 was

positioned behind the target in the beam; it detected kaons that did not interact in the target.

The scattered particles were detected by means of scintillator counter hodoscopes placed on a circle with radius 56 cm around the target; they recorded the polar and azimuthal coordinates of the scattered kaon and the recoil proton. Looking downstream, 24 polar counters are placed to the left, 22 to the right of the beam. Most scintillators were 4 cm wide, 5 mm thick, and 21 cm high. As shown in Fig. 1, a few counters in the backward region were broader; however, they span nearly the same interval in $\cos \vartheta_{c.m.}$ as the others.

The azimuthal angle hodoscopes are shaped like "orange peels", i.e. the vertical size at each laboratory angle ϑ was proportional to $\sin \vartheta$, with the result that the azimuthal angular acceptance was almost independent of ϑ. On each side there were five azimuthal counters, 135 cm long, 5 mm thick, maximum vertical size 4 cm, and shaped as indicated in Fig. 1. In this way the five coplanar combinations of a left and a right azimuthal counter corresponded each to a 4° rotation of the scattering plane around the incident beam axis. The total azimuthal acceptance angle of the counters was thus restricted to ±10° around the horizontal scattering plane. The correction to the polarization due to the inclination of the scattering plane has been neglected.

The forward tips of these large azimuthal counters could not be made 100% efficient due to the unfavourable light collection to the photomultipliers which are mounted at 90° to the scintillator planes. For this reason the tips (out to 30° left, 20° right) of these counters were doubled with small counters of identical shape.

Two counters (P_1 and P_2) were placed directly above and below the target, approximately covering the pole faces; they were designed in such a way as to fill up as much as possible the solid angle not seen by the hodoscopes. In anticoincidence, they rejected events accompanied by other particles (or gammas) that were detected in either of these two counters.

Finally, three 2 × 2 × 2 mm scintillators, not shown in Fig. 1, have been used to scan the size and the angular divergence of the beam and to

check the deflection through the magnetic field of the target. They were placed in front of C_1, near B_3, and 50 cm behind B_5.

2.5 Electronics

The description of the counter arrangement in Section 2.4 led to the following conditions to be fulfilled by an event in order to be accepted for further analysis:

i) a beam telescope trigger ($B_1\ \bar{C}_2\ B_2\ B_3\ \bar{B}_4\ \bar{B}_5$) produced by a kaon interacting in the target: for data above 2.2 GeV/c an additional coincidence with C_1 was required;

ii) a hodoscope trigger, which required that one and only one secondary particle hits the polar as well as the azimuthal hodoscopes at each side of the beam;

iii) an anticoincidence from the pole face counters which guaranteed that an apparently good event was not accompanied by a charged particle outside the solid angle subtended by the hodoscopes.

No conditions have been set on the nature or on the degree of coplanarity of the two secondary particles. Both conditions have been imposed in the off-line computer analysis of the events (see Section 3).

If an event satisfied conditions (i), (ii) and (iii) above, a transfer to magnetic tape was initiated. This consisted of reading out all nine "pattern units" containing the information from the hodoscopes, the number of focused kaons and interacting kaons which had occurred since the previous event was transferred, the target polarization which was measured and entered into a binary scaler once per PS burst, and some identifying constants. During a transfer, which took about 20 msec per event, the entire electronics was kept closed by a system of bistable circuits, in order to avoid dead-time corrections caused by the tape transfer. In addition, the signals from the polar counters were fed into a 32 × 32 matrix and scope display unit. Pulse lengths were 20 nsec throughout the fast logic system.

2.6 Data acquisition

In the data-taking phase, the total beam intensity (pions for more than 95%) was at all momenta kept below 4×10^5 per (200 msec) burst.

This implies that above 2 GeV/c the available rate had to be reduced by adjusting the mass and momentum slits. This limitation in the speed of data-taking was imposed by two factors. One was the dead-time losses in the beam telescope that were about 10% at the above-mentioned counting rate, while the second was the spurious setting of bits in the pattern units. These pattern units were gated on for 30 nsec per event. During part of this time, a spurious count in any of the hodoscope counters not fired by the event could set the bit pattern corresponding to the counter number and could thus turn the event into an inelastic event, since seemingly more than one secondary went into one of the hodoscopes. About 4% of the elastic events were spoiled by this effect in agreement with the amount expected from the measured single rates in the hodoscope counters at a beam rate of 4×10^5. For the total rate limited to 4×10^5 per burst, the focused kaon rates obtained at various momenta were always between 3,000 and 10,000 per burst, resulting in an average counting rate of 1 to 3 events per burst. At each momentum, about 50,000 events (as defined in Section 2.4) were collected in 50 hours at a rate of 8,000-15,000 events per tape reel. After every 12,500 events the target polarization was reversed.

Visual monitoring during the data-taking was provided by the matrix and display unit, which showed left/right coincidences between polar counters; the free hydrogen peak was clearly visible and some failures in the electronics could easily be spotted this way.

The events were processed through a chain of programmes to be discussed in the next section. The first two of these programmes were run every 12 hours during the data-taking phase of the experiment in order to check the performance of the counters, the distribution of events over the various coplanarity conditions, the fraction of inelastic or spoiled events, etc. This feed-back between computer and apparatus was indispensable for efficient running of the experiment.

3. DATA REDUCTION

3.1 The coplanarity conditions

Approximately 10^6 events as defined by the trigger conditions were collected on a total of 150 magnetic tapes. In order to condense this

information into a form more convenient for further analysis, a first programme*) decoded the events, eliminated spoiled elastic events which the electronic vetos failed to reject as described in Section 2.5 and kept a record of the performance of the counters. The information was compressed onto 10 magnetic tapes for subsequent analysis.

The four coordinates recorded for each event (two azimuthal plus two polar angles) determine in principle a $5 \times 5 \times 22 \times 24$ matrix with 13,200 channels. However, many channels are equivalent, since the inclination of the scattering plane can be disregarded, and since only differences between the azimuthal angles of the secondary particles need to be distinguished. One is then left with a $5 \times 22 \times 24$ matrix in which the first axis now refers to the five differences in azimuthal angle which can be defined with the given set of counters.

The full lines in Fig. 2 show a cut at the left-hand polar counter No. 4 through the matrix of events obtained at 1.63 GeV/c. A peak appears, mainly amongst events with small or no difference in azimuthal angle between the scattered kaon and the recoil proton. This peak is due to recoil protons from scattering on free hydrogen in the target, in coincidence with kaons scattered to the left into counter No. 4. The apparent non-coplanarity for part of the hydrogen events is due to the size of the target, and to a lesser extent to multiple scattering of the secondaries in the target.

3.2 Background subtraction, normalization

The simplest way of determining the background is to collect data with a dummy target at each incident momentum. However, this would double the beam time needed for the experiment, since at least the same statistics are required as for the polarized target runs. We have therefore performed dummy target measurements at only two momenta, 1.63 GeV/c and 1.98 GeV/c, and we employed the non-coplanar events of the polarized target runs to subtract the background, using the dummy target data to check the procedure.

---

*) The various analysis programmes have been run on CDC 6600, CDC 6400, CDC 3800 and IBM 1800 computers.

Figures 2 and 3 give a comparison of the two different spectra obtained at 1.63 GeV/c. In both drawings the solid lines refer to the polarized target spectrum while the dots refer to the corresponding results of the dummy target run. In Fig. 2 we see that beyond the elastic peak the distribution of the events from the polarized target and the dummy target is equal in the polar as well as in the azimuthal angle direction. A slight enhancement occurs in the background under the elastic peak. This is due to the contribution of elastic scattering of kaons on bound protons. Figure 3 shows the sum of the coplanar and near coplanar events (first two graphs of Fig. 2) together with the normalized sum of the lower three graphs of Fig. 2 for the polarized target case (dotted line). The agreement between the two background spectra obtained is very good. We made the same comparison at 1.98 GeV/c and found that there is no energy dependence in the normalization factors to be applied in the procedure.

As the background spectrum was seen to change very slowly with energy, the background data at neighbouring energies could be combined, so that the background statistics were generally better than the statistics of the data. Even so, cross-sections of less than 100 μb are poorly determined due to the very unfavourable ratio of elastic to background events. As a final check we compared the shape of the angular distributions obtained with available data from the literature (Ref. 1).

The normalizations necessary for combining runs at various stages of the data reduction were performed by scaling via the total number of recorded events. This can result in a net asymmetry, arising from the difference in angular acceptance for the two cases: kaon scattered left, and kaon scattered right. Detailed checks have shown that the resulting asymmetry is well below 1%.

3.3 Identification of the elastic peaks

The experiment was simulated by a Monte Carlo calculation to predict the position and the width of the correlation peaks (e.g. Fig. 3) and to determine the solid angle acceptance and the centre-of-mass scattering angle $\vartheta_{c.m.}$ of the counters. Specific parameters in this calculation were the multiple scattering and energy loss in the target

assembly, the distribution of interaction points through the target, the spread in momentum and angle of the incident beam, the bending of the particles in the field, and the decay of scattered kaons.

Figure 4 shows a comparison between the Monte Carlo events and the background corrected experimental data for left polar counter No. 6 at 1.48 GeV/c. The agreement between the two spectra is equally good at all other combinations. For most purposes, a simplified but faster calculation gave adequate accuracy, although details about target and beam were omitted.

Not all peaks are amenable to a unique transformation to the centre-of-mass system. Figure 5 shows a scattering diagram in which the bands for elastic and reverse elastic scattering are indicated. The two peaks merge completely in the region beyond counter No. 13, so that no single c.m. angle can be allocated. In terms of $\cos \vartheta_{c.m.}$, the peaks are separated from +0.92 to -0.23 for the kaons going left, and from -0.96 to +0.32 for the kaon going right. The region between +0.32 and -0.23 is thus measured twice. The size of this region of overlap depends slightly on the incident momentum.

4. RESULTS

4.1 Polarizations and differential cross-sections

The results on polarizations and differential cross-sections are presented in Tables 1 to 10. Figures 6 to 11 show the differential cross-sections and the corresponding polarizations at all momenta (except 2.37 GeV/c). In the figures, the data points with spacing less than 0.035 in $\cos \vartheta_{c.m.}$ have been replaced by their weighted averages.

The polarization P has been calculated at each angle from the formula $PP_T = (U - D)/(U + D - B)$, where U(D) are the normalized number of counts before background subtraction in the elastic peak with target spin up (down); B is the normalized background, and P_T is the target polarization. In determining the sign of P, the Basel Convention*) has been followed. The angular range covered by the polarization data is from

*) The polarization is positive if, for target spin up, the incident particle is preferentially scattered to the left, looking along the downstream direction of the incident beam.

+0.92 to -0.85 in $\cos \vartheta_{c.m.}$. For the differential cross-section data, the angular range is somewhat more restricted. This is because in evaluating the rates in the most forward direction large corrections are necessary as a consequence of the loss of slow, large-angle protons in the target assembly. The steep variation of the cross-section with angle in this region makes these corrections too strongly dependent on details of beam and target assembly to be reliably represented by the Monte Carlo calculations. We have therefore rejected the forward points of the differential cross-sections and replaced them by suitably interpolated liquid-hydrogen bubble chamber data, taken from Ref. 1. The polarization data are not affected by these corrections. In this way, simultaneous fits to the differential cross-sections and polarizations can be made also in the near forward direction, a point of importance for further analysis of the data. In Tables 1 to 10 the column "sigma 1" includes these substituted points; in column "sigma 2" the corresponding polarized target points are indicated in brackets. An error of 20% has been assigned to the substituted points to account for systematic errors in the interpolation procedure.

The conversion of the angular distribution data to mb/sr has been made via the optical theorem, the total cross-section data of Ref. 2, and the assumption that the real part of the forward scattering amplitude can be neglected. The point at 0° required for this conversion was obtained from the Legendre expansion for the chosen order of fit (see below). The scale error associated with the error in the zero degree point derived from the fit is about ±8%; this error is not included in the tables and the figures.

The angular distributions show strong diffraction peaks of roughly constant slope on a t scale (momentum transfer squared), followed by a dip and a secondary maximum. Beyond the secondary maximum, the cross-sections vary in a way which shows no particular regularity with momentum. In some cases there is a second dip (e.g. 1.48, 1.73 GeV/c); in others the distributions remain more or less flat (e.g. 1.43, 1.63, 1.78 GeV/c) or drop in the backward region (in particular at the highest momenta 2.33, 2.37 GeV/c).

The polarizations are all positive and large in the region of the diffraction peaks, and go through zero at values of cos $\vartheta_{c.m.}$ near those corresponding to the first dip in the angular distributions. They reach large negative values in the central part of the angular distribution, and generally cross the zero line at least once again in the very poorly determined backward region.

The value of t at the first dip is independent of momentum; its average value over the 19 momenta is $t_{DIP} = 0.77 \pm 0.03$ (GeV/c)^2. The value of t at the first zero crossing of the polarization curves is also independent of momentum, and averages to $t_{P=0} = 0.80 \pm 0.05$ (GeV/c)^2. Hence "dip" and "zero crossing" coincide within errors.

4.2 Expansion in Legendre polynomials

The data have been parametrized by means of the Legendre polynomial expansion

$$\frac{d\sigma}{d\Omega} = \lambda\!\!\!^{-2} \sum_{\ell} A_\ell P_\ell(\cos \vartheta_{c.m.}) \qquad (1)$$

$$\vec{P} \frac{d\sigma}{d\Omega} = \hat{n}\, \lambda\!\!\!^{-2} \sum_{\ell} B_\ell P^1_\ell (\cos \vartheta_{c.m.}) . \qquad (2)$$

Here, $P_\ell(\cos \vartheta_{c.m.})$ are Legendre polynomials, $P^1_\ell(\cos \vartheta_{c.m.})$ first associated Legendre polynomials, $\lambda\!\!\!^{-}$ the c.m. wavelength divided by 2π, $\cos \vartheta_{c.m.} = \vec{k}_i \cdot \vec{k}_f / |k_i| \cdot |k_f|$ and $\hat{n} = \vec{k}_i \times \vec{k}_f / |k_i \times k_f|$; $\vec{k}_i$, $\vec{k}_f$ are the initial, resp. final momenta of the kaon in the c.m. system. The order of the fit is determined by the onset of stability in A_ℓ and B_ℓ as a function of the order of fit; this generally coincides with a sudden decrease in χ^2. The order of fit for the B coefficients is lower than the one for the A coefficients, reflecting the fact that the polarization data have larger errors and are thus adequately described by less terms in the Legendre expansion. Tables 11 to 48 show the A and B coefficients as obtained from the normalized data as given in Tables 1 to 10 for four orders of fit: the chosen one (underlined) plus three others nearby. Figures 13 and 14 show the A and the B coefficients obtained from the present experiment.

4.3 Discussion of the results

The most striking feature of the A coefficients is a generally steep increase with increasing energy, while Fig. 12 shows that $\sigma_{el} = 4\pi\lambda^2 A_0$ and $\sigma_{tot} = 4\pi\lambda^2(\Sigma A_\ell)^{1/2}$ decrease slowly through the range of momenta covered by this experiment. This suggests a dominance of diffraction-like background waves over the possibly present resonance contributions. This behaviour is in marked contrast to $K^-p \to \bar{K}^0n$ data[8] in this range of momenta, in which in particular the lower A coefficients are about constant, or even drop with increasing momentum; apparently, the background waves are distributed about equally over both I-spin channels, which largely cancel in $K^-p \to \bar{K}^0n$ but not in $K^-p \to K^-p$.

Another feature of the A coefficients is the absence, in the 1.4-2.4 GeV/c region, of any pronounced structure in the lower coefficients. This is in contrast with the structure present around 1 GeV/c where the highly elastic $Y^*(1765)$ and $Y^*(1820)$ are located. It thus seems probable that whatever resonances may be present in the 1.4-2.4 GeV/c region, they have small elasticities.

The coefficients A_5, A_6 (and perhaps A_4 also) show a bump superimposed on the over-all rising trend in these coefficients between $\sim$ 1.5 and $\sim$ 1.8 GeV/c, where the $Y^*(2035)$ and $Y^*(2100)$ occur. In A_7 the strong increase in background waves only sets in at $\sim$ 1.9 GeV/c, suggesting that the bump in A_7 below 1.9 GeV/c is due to two interfering $7/2$ waves of opposite parity only. The pattern of A_8 and A_9, which are non-zero only above $\sim$ 2 GeV/c, confirms that $9/2$ waves do not seem to be important below this momentum.

The lower B coefficients, in particular B_1, decrease with increasing momentum towards a minimum around 1.7-1.8 GeV/c and then increase again; the higher B coefficients (B_4, B_5) are less dependent on momentum below 1.8 GeV/c, but from there on show roughly the same increase with momentum as the lower coefficients. The contribution of the lower partial waves, to which the tails of $Y^*(1765)$ and $Y^*(1800)$ contribute significantly, is thus decreasing, while above $\sim$ 1.9 GeV/c the partial waves with higher angular momenta set in; hence a minimum in the lower B's and an initially flat, then rising behaviour in the higher B's.

Figure 15 shows the behaviour of the polarization at cos $\vartheta_{c.m.} = 0$ as a function of incident momentum. Two distinct bumps appear, which can be easily identified with the recently discovered $Y_1^*(2030\ \text{MeV})$ and $Y_0^*(2100\ \text{MeV})$ resonances (Ref. 2). Possibly as a result of interference effects, the two resonances appear here as separate bumps, while in the total cross-section data they could only be disentangled by separating the two isospin channels. Wohl et al.[8] conclude from the charge exchange data that the assignments $7/2^+$ and $7/2^-$ for the 2030 and the 2100 MeV resonances are most probable. As mentioned above, the behaviour of the A_7 coefficient in our data in the region of these two resonances also suggests an interference of two $7/2$ waves in accordance with this assignment.

To arrive at quantitative conclusions concerning resonances, a more detailed knowledge of the background waves is required than can be obtained from an inspection of the trends in A and B coefficients alone. This is particularly the case above ~ 2 GeV/c where resonance effects only appear in interference with background waves. We defer a discussion of background-resonance interference to a later paper[9], where specific diffraction models will be discussed.

Acknowledgements

We wish to thank Mr. M. Arbet for his able assistance in the course of this experiment. We are very much indebted to Messrs. M. Borghini, J. Conciencia, O. Runolfsson, M. Uldry, and J. Vermeulen for setting up and maintaining the polarized target; their untiring and competent assistance has been a vital element in the running of the experiment. We thank Mr. S. Andersson and Mr. G. Plaut for their contributions to the analysis of the data.

We are pleased to acknowledge the support given to the experiment by Professors W. Paul, P. Preiswerk and A.H. Wapstra. This work was supported in part by the Stichting voor Fundamenteel Onderzoek der Materie (F.O.M.), which is supported by the Nederlandse Organisatie von Zuiver Wetenschappelijk Onderzoek (Z.W.O.).

REFERENCES

1) A. Fridman, O. Benary, A. Michalon, B. Schiby, R. Strub and G. Zech, Phys.Rev. 145, 1136 (1966);
R. Crittenden, H.J. Martin, W. Kernan, L. Leipuner, A.C. Li, F. Ayer, L. Marshall and M.L. Stevenson, Phys.Rev.Letters 12, 429 (1964).
M. Dickinson, S. Miyashita, L. Marshall Libby and P. Kearney, Phys.Letters 24B, 596 (1967).
J.R. Ficenec and W.O. Trower, Phys.Letters 25B, 369 (1967).
G.R. Lynch, private communication.

2) R. Cool, G. Giacomelli, T.F. Kycia, B.A. Leontic, K.K. Li, A. Lundby and J. Teiger, Phys.Rev.Letters 17, 102 (1966).
R.J. Abrams, R.L. Cool, G. Giacomelli, T.F. Kycia, B.A. Leontic, K.K. Li and D.N. Michael, Phys.Rev.Letters 19, 259 (1967).
D.V. Bugg et al., Rutherford-Birmingham-Cambridge collaboration preprint 1967.

3) J. Mayer, Rapporteur talk in Proc. Heidelberg Int.Conf. on Elementary Particles, 1967 (North-Holland Publ. Co., 1967), p.117.

4) G. Brautti, G. Fidecaro, T. Massam, M. Morpurgo, Th. Muller, G. Petrucci, E. Rocco, P. Schiavon, M. Schneegans and A. Zichichi, Nuovo Cimento 38, 1861 (1965).

5) M. Borghini, P. Roubeau and C. Ryter, Nucl.Instrum.Meth. 49, 248 (1967).
M. Borghini, P. Roubeau and C. Ryter, Nucl.Instrum.Meth. 49, 259 (1967).

6) M.B. Watson, M. Ferro-Luzzi and R.D. Tripp, Phys.Rev. 131, 2248 (1963).
P. Bastien and J.P. Berge, Phys.Rev.Letters 10, 188 (1963).
W.R. Holley, E.F. Beall, D. Keefe, L.T. Kerth, J.J. Thresher, C.L. Wang and W.A. Wenzel, Phys.Rev. 154, 1273 (1967).
G.R. Lynch, private communication.
N.M. Gelfand, D. Harmsen, R. Levi Setti, M. Raymund, J. Dolde and W. Männer, XIIIth Int.Conf. on High-Energy Physics, Berkeley (1966).

7) C.R. Cox, K.S. Heard, J.C. Sleeman, P.J. Duke, R.E. Hill, W.R. Holley, D.P. Jones, J.J. Thresher, F.C. Shoemaker and J.B. Warren, reported in Ref. 3.

8) C.G. Wohl, F.T. Solmitz and M.L. Stevenson, Phys.Rev.Letters 17, 107 (1966).

9) C. Daum, F. Erné, J.P. Lagnaux, J.C. Sens, M. Steuer and F. Udo, to be published.

TABLE CAPTIONS

Tables 1 to 10:

K^-p polarization and differential cross-section data with errors. The column "sigma 1" contains the differential cross-sections in mb/sr, while the column "sigma 2" contains the original forward cross-section points rejected because of efficiency uncertainties. The uncertainty of ±8% due to the conversion of the differential cross-sections to mb/sr is not included in the errors.

Tables 11 to 29:

Coefficients A_ℓ from the Legendre expansion of the differential cross-section data (formula 1). The chosen order is underlined. Three orders nearby are given for comparison. $P(\chi^2)$ is the probability of fit calculated from χ^2 and the number of degrees of freedom. σ_{tot} and σ_{el} are respectively the total cross-section and the total elastic cross-section calculated from the fit. As a result of the normalization procedure applied to the data, the σ_{tot} calculated from the fit for the chosen order coincides with the literature value. Units: sr^{-1}.

Tables 30 to 48:

Coefficients B_ℓ from the Legendre expansion of $P(d\sigma/d\Omega)$ according to formula 2 for four orders of fit. The chosen order is underlined. $P(\chi^2)$ is the probability of fit calculated from χ^2 and the number of degrees of freedom. The unit is sr^{-1}.

Table 1

INCIDENT MOMENTUM =1383.0 MEV/C
CENTER OF MASS MOMENTUM= 658.8 MEV/C

COS	POL	DPOL	SIGMA(1)	DSIGMA(1)	SIGMA(2)	DSIGMA(2)
0.898	0.25	0.54	4.492	0.898	(5.937)	(3.541)
0.855	0.27	0.08	3.605	0.721	(2.166)	(0.206)
0.765	0.32	0.07	1.988	0.178		
0.659	0.63	0.08	1.349	0.120		
0.541	0.37	0.12	0.751	0.073		
0.417	0.80	0.16	0.398	0.049		
0.385	0.56	0.21	0.334	0.052		
0.290	0.26	0.23	0.244	0.041		
0.262	0.39	0.22	0.271	0.044		
0.162	-0.12	0.34	0.158	0.040		
0.129	-0.02	0.21	0.262	0.041		
0.039	-0.91	0.34	0.192	0.045		
-0.012	-1.12	0.33	0.139	0.031		
-0.080	-0.33	0.23	0.297	0.051		
-0.160	-0.47	0.19	0.280	0.040		
-0.191	-0.95	0.22	0.369	0.059		
-0.295	-0.22	0.27	0.315	0.064		
-0.310	-0.86	0.20	0.271	0.040		
-0.457	0.13	0.22	0.238	0.040		
-0.596	0.16	0.17	0.348	0.047		
-0.723	0.45	0.18	0.420	0.057		
-0.830	-0.16	0.49	0.123	0.045		
-0.913	-0.10	0.54	0.216	0.085		

INCIDENT MOMENTUM =1433.0 MEV/C
CENTER OF MASS MOMENTUM= 674.9 MEV/C

COS	POL	DPOL	SIGMA(1)	DSIGMA(1)	SIGMA(2)	DSIGMA(2)
0.901	-0.14	0.37	3.630	0.726	(4.087)	(1.808)
0.856	0.30	0.07	2.759	0.552	(1.866)	(0.172)
0.765	0.42	0.08	1.549	0.310	(1.372)	(0.127)
0.658	0.66	0.10	0.797	0.077		
0.540	0.95	0.15	0.447	0.051		
0.414	0.91	0.18	0.275	0.037		
0.392	0.90	0.26	0.214	0.039		
0.286	0.01	0.21	0.213	0.033		
0.270	0.01	0.21	0.215	0.034		
0.158	-0.19	0.43	0.097	0.031		
0.137	-0.48	0.28	0.145	0.030		
0.034	-0.34	0.38	0.123	0.034		
-0.004	-1.05	0.31	0.114	0.024		
-0.086	-1.47	0.41	0.152	0.037		
-0.153	-0.95	0.24	0.177	0.029		
-0.197	-0.58	0.20	0.309	0.047		
-0.300	-0.39	0.23	0.309	0.052		
-0.303	-0.70	0.20	0.207	0.031		
-0.451	-0.11	0.21	0.197	0.031		
-0.592	-0.10	0.22	0.197	0.033		
-0.720	0.07	0.18	0.303	0.043		
-0.828	0.15	0.24	0.218	0.040		
-0.912	-0.53	0.55	0.202	0.078		

Table 2

INCIDENT MOMENTUM =1483.0 MEV/C
CENTER OF MASS MOMENTUM= 690.8 MEV/C

COS	POL	DPOL	SIGMA(1)	DSIGMA(1)	SIGMA(2)	DSIGMA(2)
0.903	-0.02	0.24	3.940	0.788	(5.729)	(1.926)
0.859	0.20	0.07	3.055	0.611	(2.062)	(0.185)
0.765	0.40	0.07	1.578	0.137		
0.657	0.73	0.10	0.732	0.073		
0.537	1.00	0.16	0.263	0.033		
0.411	1.15	0.26	0.180	0.033		
0.399	1.01	0.26	0.173	0.032		
0.281	0.25	0.32	0.124	0.030		
0.277	-0.26	0.31	0.110	0.025		
0.153	-0.69	0.68	0.064	0.030		
0.145	-0.22	0.24	0.144	0.026		
0.028	-0.96	0.38	0.169	0.042		
0.003	-1.03	0.30	0.143	0.029		
-0.091	-0.96	0.32	0.177	0.038		
-0.146	-1.19	0.22	0.210	0.031		
-0.202	-0.86	0.28	0.226	0.044		
-0.297	-0.53	0.17	0.215	0.029		
-0.304	-0.78	0.24	0.311	0.052		
-0.446	-0.22	0.23	0.150	0.026		
-0.588	0.41	0.27	0.155	0.032		
-0.707	0.59	0.22	0.247	0.041		
-0.827	0.04	0.18	0.328	0.045		
-0.911	-0.06	0.76	0.128	0.073		

INCIDENT MOMENTUM =1534.0 MEV/C
CENTER OF MASS MOMENTUM= 706.7 MEV/C

COS	POL	DPOL	SIGMA(1)	DSIGMA(1)	SIGMA(2)	DSIGMA(2)
0.905	0.04	0.16	4.428	0.886	(6.531)	(1.806)
0.858	0.18	0.06	3.100	0.620	(2.370)	(0.201)
0.765	0.28	0.07	1.538	0.132		
0.656	0.74	0.11	0.638	0.065		
0.535	0.88	0.20	0.190	0.028		
0.407	1.11	0.39	0.111	0.028		
0.284	0.55	0.43	0.081	0.025		
0.277	0.54	0.34	0.110	0.027		
0.152	-0.35	0.36	0.083	0.022		
0.148	-1.20	0.55	0.085	0.028		
0.023	-0.73	0.32	0.151	0.034		
0.010	-1.19	0.29	0.148	0.028		
-0.097	-0.77	0.26	0.155	0.029		
-0.138	-0.97	0.22	0.186	0.028		
-0.208	-0.51	0.20	0.307	0.045		
-0.290	-0.49	0.20	0.150	0.023		
-0.310	-0.86	0.29	0.241	0.048		
-0.440	-0.78	0.24	0.164	0.028		
-0.583	0.32	0.28	0.139	0.029		
-0.714	0.58	0.26	0.192	0.036		
-0.829	0.17	0.23	0.224	0.038		
-0.910	-0.66	0.57	0.149	0.059		

Table 3

INCIDENT MOMENTUM =1584.0 MEV/C
CENTER OF MASS MOMENTUM= 722.0 MEV/C

COS	POL	DPOL	SIGMA(1)	DSIGMA(1)	SIGMA(2)	DSIGMA(2)
0.906	0.02	0.24	4.530	0.906	(3.377)	(1.120)
0.858	0.24	0.06	3.056	0.611	(2.320)	(0.197)
0.765	0.23	0.07	1.416	0.124		
0.654	0.58	0.12	0.520	0.057		
0.532	1.12	0.20	0.175	0.026		
0.412	1.05	0.54	0.081	0.027		
0.404	0.49	0.28	0.111	0.022		
0.292	-0.43	0.45	0.074	0.024		
0.273	-0.37	0.34	0.108	0.026		
0.159	-0.79	0.40	0.083	0.022		
0.143	-0.18	0.51	0.074	0.027		
0.017	-1.22	0.44	0.117	0.032		
0.002	-0.34	0.29	0.105	0.022		
-0.102	-0.82	0.49	0.074	0.024		
-0.131	-1.09	0.25	0.132	0.023		
-0.214	-0.46	0.27	0.200	0.039		
-0.283	-0.44	0.22	0.154	0.025		
-0.316	-1.19	0.33	0.221	0.047		
-0.434	-0.82	0.23	0.152	0.025		
-0.579	0.48	0.35	0.118	0.029		
-0.710	0.16	0.24	0.196	0.034		
-0.823	-0.12	0.25	0.197	0.036		
-0.910	-1.28	1.25	0.077	0.055		

INCIDENT MOMENTUM =1634.0 MEV/C
CENTER OF MASS MOMENTUM= 737.0 MEV/C

COS	POL	DPOL	SIGMA(1)	DSIGMA(1)	SIGMA(2)	DSIGMA(2)
0.908	0.27	0.15	5.494	1.099	(7.042)	(1.877)
0.858	0.14	0.06	3.305	0.278		
0.764	0.19	0.08	1.661	0.155		
0.653	0.52	0.15	0.519	0.065		
0.530	1.42	0.41	0.159	0.039		
0.419	0.98	0.39	0.144	0.037		
0.400	0.86	0.49	0.076	0.025		
0.298	0.08	0.51	0.081	0.030		
0.268	0.58	1.65	0.027	0.030		
0.167	-0.96	0.51	0.083	0.028		
0.137	-1.14	0.53	0.105	0.035		
0.025	-0.66	0.33	0.146	0.034		
0.011	-0.93	0.64	0.097	0.040		
-0.108	-0.53	0.41	0.115	0.033		
-0.124	-1.03	0.36	0.113	0.027		
-0.219	-1.22	0.37	0.201	0.048		
-0.277	-0.78	0.22	0.205	0.032		
-0.321	-0.93	0.46	0.187	0.057		
-0.429	-1.36	0.42	0.111	0.028		
-0.574	-0.37	0.42	0.118	0.036		
-0.707	0.21	0.34	0.163	0.040		
-0.821	-0.21	0.37	0.157	0.043		

Table 4

INCIDENT MOMENTUM =1684.0 MEV/C
CENTER OF MASS MOMENTUM= 751.8 MEV/C

COS	POL	DPOL	SIGMA(1)	DSIGMA(1)	SIGMA(2)	DSIGMA(2)
0.909	0.33	0.20	4.869	0.974	(3.297)	(0.973)
0.859	0.26	0.06	3.146	0.629	(2.697)	(0.232)
0.764	0.36	0.07	1.538	0.137		
0.651	0.46	0.14	0.495	0.060		
0.527	-0.03	0.28	0.164	0.034		
0.425	0.12	0.37	0.117	0.032		
0.396	0.50	0.35	0.124	0.031		
0.305	0.10	0.30	0.147	0.033		
0.263	0.17	0.39	0.105	0.031		
0.174	-0.33	0.26	0.156	0.031		
0.132	-0.93	0.33	0.155	0.035		
0.032	-1.17	0.41	0.094	0.025		
0.006	-0.98	0.42	0.130	0.037		
-0.114	-1.66	0.72	0.100	0.039		
-0.117	-0.94	0.35	0.119	0.029		
-0.225	-0.68	0.36	0.147	0.038		
-0.270	-0.59	0.22	0.171	0.028		
-0.327	-0.63	0.46	0.154	0.050		
-0.423	-1.07	0.43	0.088	0.025		
-0.570	-0.04	0.53	0.061	0.024		
-0.704	0.00	0.56	0.083	0.035		
-0.819	-0.56	1.03	0.046	0.033		
-0.908	0.25	1.36	0.052	0.053		

INCIDENT MOMENTUM =1734.0 MEV/C
CENTER OF MASS MOMENTUM= 766.3 MEV/C

COS	POL	DPOL	SIGMA(1)	DSIGMA(1)	SIGMA(2)	DSIGMA(2)
0.912	0.07	0.13	5.208	1.042	(4.651)	(1.206)
0.859	0.21	0.05	3.385	0.677	(3.247)	(0.254)
0.763	0.48	0.09	1.476	0.295	(1.009)	(0.099)
0.649	0.32	0.11	0.603	0.060		
0.524	0.48	0.26	0.164	0.029		
0.431	-0.23	0.28	0.143	0.029		
0.392	-0.73	0.50	0.076	0.026		
0.312	-0.13	0.23	0.158	0.027		
0.258	-0.87	0.25	0.124	0.022		
0.181	-0.89	0.24	0.138	0.024		
0.127	-0.91	0.40	0.104	0.028		
0.040	-0.76	0.20	0.164	0.024		
0.000	-1.06	0.36	0.132	0.031		
-0.110	-0.62	0.19	0.185	0.027		
-0.120	-1.32	0.48	0.116	0.034		
-0.231	-0.90	0.28	0.149	0.030		
-0.264	-0.78	0.23	0.121	0.020		
-0.417	-0.52	0.20	0.164	0.024		
-0.565	-0.67	0.58	0.049	0.020		
-0.701	0.96	0.55	0.072	0.024		
-0.817	-0.27	0.42	0.123	0.037		
-0.907	-0.72	0.53	0.135	0.050		

Table 5

INCIDENT MOMENTUM =1784.0 MEV/C
CENTER OF MASS MOMENTUM= 780.6 MEV/C

COS	POL	DPOL	SIGMA(1)	DSIGMA(1)	SIGMA(2)	DSIGMA(2)
0.914	0.00	0.09	5.158	1.031	(5.063)	(1.230)
0.859	0.08	0.05	3.225	0.646	(2.893)	(0.221)
0.762	0.22	0.06	1.542	0.127		
0.647	0.33	0.11	0.521	0.053		
0.521	0.91	0.27	0.149	0.027		
0.437	-0.86	0.30	0.121	0.025		
0.387	0.53	0.64	0.056	0.024		
0.319	-0.30	0.21	0.161	0.025		
0.253	-0.85	0.33	0.090	0.020		
0.188	-0.57	0.21	0.153	0.023		
0.121	-0.93	0.31	0.089	0.019		
0.046	-0.52	0.25	0.114	0.021		
-0.006	-0.64	0.39	0.100	0.027		
-0.103	-0.82	0.25	0.127	0.022		
-0.126	-1.28	0.63	0.079	0.029		
-0.237	-0.34	0.42	0.111	0.033		
-0.257	-0.80	0.28	0.092	0.018		
-0.338	-0.87	0.39	0.147	0.038		
-0.422	-0.89	0.23	0.134	0.022		
-0.561	-0.63	0.33	0.093	0.021		
-0.697	-0.15	0.53	0.056	0.021		
-0.814	-0.11	0.30	0.164	0.035		
-0.905	-0.98	0.79	0.075	0.037		

INCIDENT MOMENTUM =1884.0 MEV/C
CENTER OF MASS MOMENTUM= 808.6 MEV/C

COS	POL	DPOL	SIGMA(1)	DSIGMA(1)	SIGMA(2)	DSIGMA(2)
0.916	0.08	0.10	6.055	1.211	(4.920)	(1.220)
0.859	0.20	0.05	3.512	0.272		
0.760	0.38	0.07	1.498	0.133		
0.643	0.39	0.12	0.507	0.055		
0.514	1.28	0.43	0.109	0.028		
0.379	0.93	0.76	0.058	0.028		
0.332	-0.47	0.40	0.097	0.027		
0.243	-0.93	0.40	0.117	0.030		
0.202	-0.38	0.26	0.140	0.026		
0.110	-0.47	0.31	0.109	0.024		
0.061	-0.37	0.22	0.185	0.030		
-0.018	-0.51	0.32	0.150	0.033		
-0.089	-0.85	0.46	0.068	0.020		
-0.138	-1.34	0.74	0.085	0.035		
-0.245	-0.39	0.31	0.109	0.024		
-0.249	-0.86	0.51	0.122	0.040		
-0.401	-0.87	0.29	0.127	0.024		
-0.552	-0.33	0.34	0.094	0.023		
-0.691	-0.73	0.39	0.088	0.023		
-0.811	0.84	0.63	0.092	0.037		

Table 6

INCIDENT MOMENTUM =1934.0 MEV/C
CENTER OF MASS MOMENTUM= 822.3 MEV/C

COS	POL	DPOL	SIGMA(1)	DSIGMA(1)	SIGMA(2)	DSIGMA(2)
0.917	0.26	0.09	5.134	1.027	(2.644)	(0.644)
0.859	0.23	0.05	2.981	0.596	(1.984)	(0.150)
0.759	0.29	0.04	1.326	0.097		
0.641	0.52	0.10	0.323	0.031		
0.511	0.54	0.25	0.085	0.015		
0.375	-0.12	0.37	0.054	0.014		
0.237	-0.54	0.30	0.072	0.015		
0.104	-0.38	0.23	0.106	0.017		
-0.024	-0.51	0.28	0.066	0.013		
-0.144	-0.61	0.37	0.072	0.018		
-0.238	-0.33	0.26	0.065	0.012		
-0.255	0.43	0.44	0.065	0.020		
-0.355	-0.66	0.44	0.057	0.017		
-0.395	-0.41	0.29	0.056	0.012		
-0.547	-0.01	0.18	0.099	0.013		
-0.687	-0.59	1.20	0.016	0.013		
-0.903	-0.20	2.61	0.011	0.020		

INCIDENT MOMENTUM =1984.0 MEV/C
CENTER OF MASS MOMENTUM= 835.8 MEV/C

COS	POL	DPOL	SIGMA(1)	DSIGMA(1)	SIGMA(2)	DSIGMA(2)
0.918	0.14	0.09	5.344	1.072	(3.745)	(0.906)
0.859	0.19	0.05	2.943	0.223		
0.758	0.27	0.07	1.083	0.093		
0.639	0.47	0.11	0.400	0.040		
0.508	0.96	0.34	0.113	0.024		
0.461	-0.56	0.60	0.051	0.021		
0.371	-0.21	0.48	0.058	0.020		
0.344	-0.17	0.24	0.123	0.021		
0.233	-0.77	0.29	0.111	0.022		
0.215	-0.39	0.21	0.130	0.020		
0.098	-0.67	0.23	0.150	0.025		
0.074	-0.61	0.22	0.113	0.018		
-0.030	-1.05	0.36	0.073	0.018		
-0.076	-0.28	0.25	0.106	0.019		
-0.150	-0.37	0.64	0.053	0.024		
-0.232	-0.57	0.29	0.071	0.015		
-0.260	-0.94	0.48	0.086	0.027		
-0.360	-1.07	0.46	0.077	0.023		
-0.389	-0.15	0.39	0.067	0.019		
-0.542	-0.74	0.44	0.051	0.015		
-0.684	-0.90	0.88	0.032	0.018		
-0.807	0.74	0.73	0.048	0.022		

Table 9

INCIDENT MOMENTUM =2284.0 MEV/C
CENTER OF MASS MOMENTUM= 913.0 MEV/C

COS	POL	DPOL	SIGMA(1)	DSIGMA(1)	SIGMA(2)	DSIGMA(2)
0.926	0.03	0.07	5.728	1.149	(3.906)	(0.929)
0.857	0.28	0.05	2.499	0.190		
0.750	0.44	0.09	0.636	0.061		
0.624	0.83	0.22	0.151	0.024		
0.487	-0.32	0.53	0.047	0.018		
0.343	-0.36	0.22	0.126	0.021		
0.253	0.13	0.23	0.112	0.019		
0.201	-0.54	0.40	0.070	0.020		
0.114	-1.04	0.40	0.079	0.020		
0.064	-0.73	0.36	0.090	0.022		
-0.037	-0.49	0.28	0.092	0.019		
-0.066	-1.10	0.52	0.070	0.022		
-0.186	0.05	0.37	0.064	0.017		
-0.195	-0.20	1.08	0.016	0.013		
-0.357	-0.51	0.61	0.035	0.015		
-0.516	-0.10	0.50	0.045	0.017		
-0.664	-0.84	0.52	0.064	0.022		
-0.794	0.09	1.44	0.017	0.018		
-0.896	0.58	1.21	0.035	0.029		

INCIDENT MOMENTUM =2325.0 MEV/C
CENTER OF MASS MOMENTUM= 923.1 MEV/C

COS	POL	DPOL	SIGMA(1)	DSIGMA(1)	SIGMA(2)	DSIGMA(2)
0.927	0.18	0.09	4.703	0.940	(3.085)	(0.740)
0.856	0.32	0.06	1.946	0.189		
0.749	0.55	0.11	0.481	0.066		
0.622	0.99	0.54	0.061	0.020		
0.483	-0.40	0.43	0.051	0.015		
0.339	-1.12	0.44	0.043	0.012		
0.196	-0.31	0.22	0.097	0.015		
0.058	-0.95	0.28	0.105	0.019		
-0.030	-0.37	0.24	0.097	0.016		
-0.072	-1.09	0.84	0.038	0.019		
-0.189	-0.72	0.40	0.042	0.011		
-0.351	-0.44	0.65	0.027	0.012		
-0.511	1.12	0.79	0.027	0.012		
-0.661	-0.87	1.69	0.014	0.014		
-0.895	0.19	0.49	0.071	0.024		

Table 10

INCIDENT MOMENTUM =2374.0 MEV/C
CENTER OF MASS MOMENTUM= 935.1 MEV/C

COS	POL	DPOL	SIGMA(1)	DSIGMA(1)	SIGMA(2)	DSIGMA(2)
0.928	0.21	0.07	4.921	0.984	(3.475)	(0.827)
0.856	0.31	0.06	1.962	0.192		
0.748	0.63	0.11	0.492	0.058		
0.619	0.41	0.46	0.061	0.020		
0.479	0.55	0.65	0.040	0.018		
0.334	-0.06	0.32	0.088	0.020		
0.190	-0.34	0.39	0.074	0.020		
0.052	-0.67	0.31	0.111	0.023		
-0.077	-0.19	0.38	0.085	0.023		
-0.183	0.00	0.92	0.020	0.013		
-0.346	0.93	1.02	0.022	0.014		
-0.507	-0.34	0.82	0.022	0.013		
-0.790	0.75	1.02	0.018	0.012		
-0.894	-0.20	0.31	0.079	0.017		

Table 11

LEGENDRE COEFFICIENTS OF K^-p ANGULAR DISTRIBUTIONS

1.383 GeV/c				
No. of parameters	6	7	8	9
$P(\chi^2)$	8×10^{-3}	8×10^{-3}	5×10^{-3}	1.7×10^{-2}
A_0	0.89 ± 0.04	0.92 ± 0.05	0.93 ± 0.06	0.98 ± 0.06
A_1	1.56 ± 0.12	1.64 ± 0.14	1.67 ± 0.16	1.77 ± 0.17
A_2	1.74 ± 0.15	1.90 ± 0.20	1.94 ± 0.22	2.14 ± 0.24
A_3	1.47 ± 0.16	1.63 ± 0.21	1.69 ± 0.26	1.91 ± 0.28
A_4	0.58 ± 0.11	0.78 ± 0.20	0.83 ± 0.25	1.16 ± 0.28
A_5	0.22 ± 0.10	0.33 ± 0.14	0.39 ± 0.21	0.70 ± 0.25
A_6		0.13 ± 0.11	0.16 ± 0.14	0.53 ± 0.21
A_7			0.04 ± 0.11	0.26 ± 0.14
A_8				0.27 ± 0.11
A_9				
A_{10}				
σ_{el}	10.0 ± 0.5	10.4 ± 0.6	10.5 ± 0.6	11.0 ± 0.7
σ_{tot}	28.6 ± 1.4	30.5 ± 2.0	31.2 ± 2.6	35.1 ± 2.8

Table 12

LEGENDRE COEFFICIENTS OF K^-p ANGULAR DISTRIBUTIONS

1.433 GeV/c				
No. of parameters	6	7	8	9
$P(\chi^2)$	0.01	0.04	0.25	0.20
A_0	0.67 ± 0.04	0.75 ± 0.05	0.80 ± 0.06	0.80 ± 0.06
A_1	1.11 ± 0.12	1.29 ± 0.14	1.49 ± 0.15	1.49 ± 0.16
A_2	1.37 ± 0.15	1.68 ± 0.20	1.94 ± 0.21	1.94 ± 0.22
A_3	1.11 ± 0.15	1.40 ± 0.20	1.81 ± 0.24	1.81 ± 0.25
A_4	0.51 ± 0.10	0.87 ± 0.18	1.23 ± 0.21	1.24 ± 0.25
A_5	0.20 ± 0.09	0.39 ± 0.12	0.83 ± 0.18	0.83 ± 0.22
A_6		0.22 ± 0.09	0.45 ± 0.12	0.46 ± 0.19
A_7			0.28 ± 0.09	0.29 ± 0.13
A_8				0.04 ± 0.10
A_9				
A_{10}				
σ_{el}	7.2 ± 0.5	8.0 ± 0.6	8.6 ± 0.6	8.6 ± 0.61
σ_{tot}	24.0 ± 1.5	27.6 ± 1.9	31.9 ± 2.1	32.0 ± 2.5

Table 13

LEGENDRE COEFFICIENTS OF K^-p ANGULAR DISTRIBUTIONS

1.483 GeV/c				
No. of parameters	6	7	8	9
$P(\chi^2)$	0.01	0.01	0.49	0.45
A_0	0.73 ± 0.04	0.76 ± 0.04	0.88 ± 0.05	0.86 ± 0.06
A_1	1.30 ± 0.10	1.37 ± 0.13	1.77 ± 0.16	1.73 ± 0.17
A_2	1.72 ± 0.13	1.86 ± 0.18	2.35 ± 0.21	2.26 ± 0.25
A_3	1.50 ± 0.14	1.61 ± 0.18	2.37 ± 0.25	2.29 ± 0.28
A_4	0.92 ± 0.09	1.08 ± 0.17	1.68 ± 0.22	1.56 ± 0.29
A_5	0.37 ± 0.08	0.45 ± 0.11	1.20 ± 0.20	1.11 ± 0.25
A_6		0.10 ± 0.10	0.44 ± 0.12	0.32 ± 0.21
A_7			0.45 ± 0.10	0.40 ± 0.13
A_8				-0.07 ± 0.11
A_9				
A_{10}				
σ_{el}	7.53 ± 0.38	7.86 ± 0.50	9.00 ± 0.56	8.81 ± 0.62
σ_{tot}	26.2 ± 1.1	27.6 ± 1.6	34.21 ± 1.90	33.14 ± 2.53

Table 14

LEGENDRE COEFFICIENTS OF K^-p ANGULAR DISTRIBUTIONS

1.534 GeV/c				
No. of parameters	6	7	8	9
$P(\chi^2)$	0.18	0.05	0.39	0.35
A_0	0.72 ± 0.04	0.80 ± 0.05	0.90 ± 0.06	0.92 ± 0.07
A_1	1.37 ± 0.10	1.54 ± 0.13	1.89 ± 0.17	1.94 ± 0.19
A_2	1.80 ± 0.13	2.11 ± 0.19	2.56 ± 0.23	2.65 ± 0.28
A_3	1.66 ± 0.14	1.95 ± 0.19	2.57 ± 0.27	2.67 ± 0.32
A_4	1.05 ± 0.09	1.38 ± 0.17	1.92 ± 0.24	2.04 ± 0.32
A_5	0.45 ± 0.08	0.62 ± 0.11	1.21 ± 0.21	1.32 ± 0.28
A_6		0.20 ± 0.09	0.51 ± 0.13	0.62 ± 0.22
A_7			0.32 ± 0.10	0.38 ± 0.14
A_8				
A_9				
A_{10}				
σ_{el}	7.09 ± 0.36	7.82 ± 0.49	8.84 ± 0.58	9.04 ± 0.67
σ_{tot}	26.03 ± 1.02	28.76 ± 1.48	33.78 ± 1.89	34.78 ± 2.49

Table 15

LEGENDRE COEFFICIENTS OF K^-p ANGULAR DISTRIBUTIONS

1.584 GeV/c				
No. of parameters	6	7	8	9
$P(\chi^2)$	0.00	0.03	0.59	0.52
A_0	0.65 ± 0.04	0.79 ± 0.05	0.92 ± 0.06	0.92 ± 0.07
A_1	1.26 ± 0.10	1.57 ± 0.13	2.03 ± 0.18	2.03 ± 0.20
A_2	1.63 ± 0.13	2.15 ± 0.19	2.74 ± 0.24	2.73 ± 0.30
A_3	1.54 ± 0.14	2.03 ± 0.19	2.85 ± 0.28	2.84 ± 0.34
A_4	0.87 ± 0.09	1.44 ± 0.18	2.12 ± 0.25	2.10 ± 0.35
A_5	0.48 ± 0.08	0.76 ± 0.11	1.50 ± 0.22	1.49 ± 0.29
A_6		0.33 ± 0.09	0.69 ± 0.13	0.68 ± 0.24
A_7			0.40 ± 0.10	0.39 ± 0.14
A_8				-0.01 ± 0.11
A_9				
A_{10}				
σ_{el}	6.15 ± 0.34	7.38 ± 0.48	8.66 ± 0.58	8.63 ± 0.69
σ_{tot}	23.80 ± 0.99	28.29 ± 1.41	34.19 ± 1.80	34.65 ± 2.51

Table 16

LEGENDRE COEFFICIENTS OF K^-p ANGULAR DISTRIBUTIONS

1.634 GeV/c				
No. of parameters	6	7	8	9
$P(\chi^2)$	5.4×10^{-4}	5.5×10^{-2}	0.39	0.39
A_0	0.80 ± 0.04	0.94 ± 0.05	1.02 ± 0.06	1.05 ± 0.07
A_1	1.66 ± 0.12	1.91 ± 0.20	2.23 ± 0.16	2.32 ± 0.19
A_2	2.11 ± 0.14	2.70 ± 0.19	3.08 ± 0.23	3.24 ± 0.28
A_3	2.00 ± 0.16	2.42 ± 0.19	3.04 ± 0.27	3.23 ± 0.33
A_4	1.23 ± 0.10	1.94 ± 0.20	2.42 ± 0.25	2.65 ± 0.34
A_5	0.60 ± 0.10	0.88 ± 0.12	1.49 ± 0.23	1.70 ± 0.31
A_6		0.46 ± 0.11	0.75 ± 0.14	0.97 ± 0.26
A_7			0.37 ± 0.12	0.49 ± 0.16
A_8				0.13 ± 0.13
A_9				
A_{10}				
σ_{el}	7.2 ± 0.4	8.4 ± 0.5	9.2 ± 0.5	9.5 ± 0.6
σ_{tot}	26.1 ± 0.9	30.2 ± 1.2	34.2 ± 1.6	35.8 ± 2.2

Table 17

LEGENDRE COEFFICIENTS OF K^-p ANGULAR DISTRIBUTIONS

1.684 GeV/c				
No. of parameters	6	7	8	9
$P(\chi^2)$	1.1×10^{-3}	0.35	0.85	0.80
A_0	0.71 ± 0.04	0.91 ± 0.06	1.03 ± 0.07	1.03 ± 0.08
A_1	1.54 ± 0.12	2.03 ± 0.16	2.42 ± 0.21	2.43 ± 0.23
A_2	1.78 ± 0.15	2.63 ± 0.23	3.12 ± 0.29	3.14 ± 0.35
A_3	1.72 ± 0.16	2.50 ± 0.23	3.20 ± 0.33	3.22 ± 0.39
A_4	1.10 ± 0.11	2.02 ± 0.22	2.60 ± 0.30	2.62 ± 0.40
A_5	0.53 ± 0.09	1.03 ± 0.14	1.66 ± 0.26	1.68 ± 0.33
A_6		0.53 ± 0.11	0.86 ± 0.16	0.87 ± 0.28
A_7			0.34 ± 0.12	0.35 ± 0.16
A_8				0.01 ± 0.13
A_9				
A_{10}				
σ_{el}	6.14 ± 0.4	7.9 ± 0.5	8.9 ± 0.6	8.9 ± 0.7
σ_{tot}	23.5 ± 1.0	29.6 ± 1.4	33.8 ± 1.8	33.9 ± 2.4

Table 18

LEGENDRE COEFFICIENTS OF K^-p ANGULAR DISTRIBUTIONS

1.734 GeV/c				
No. of parameters	6	7	8	9
$P(\chi^2)$	0.00	0.05	0.21	0.18
A_0	0.78 ± 0.05	1.01 ± 0.08	1.14 ± 0.09	1.11 ± 0.10
A_1	1.59 ± 0.15	2.18 ± 0.20	2.57 ± 0.25	2.52 ± 0.27
A_2	1.94 ± 0.19	2.88 ± 0.29	3.39 ± 0.35	3.29 ± 0.39
A_3	1.75 ± 0.19	2.63 ± 0.28	3.33 ± 0.38	3.23 ± 0.43
A_4	1.22 ± 0.13	2.16 ± 0.25	2.74 ± 0.33	2.58 ± 0.43
A_5	0.49 ± 0.09	0.99 ± 0.15	1.61 ± 0.28	1.49 ± 0.35
A_6		0.48 ± 0.11	0.79 ± 0.16	0.65 ± 0.29
A_7			0.31 ± 0.12	0.24 ± 0.16
A_8				-0.07 ± 0.13
A_9				
A_{10}				
σ_{el}	6.48 ± 0.46	8.44 ± 0.64	9.47 ± 0.75	9.29 ± 0.81
σ_{tot}	23.21 ± 1.17	29.25 ± 1.55	33.21 ± 1.95	32.33 ± 2.54

Table 19

LEGENDRE COEFFICIENTS OF K^-p ANGULAR DISTRIBUTIONS

1.784 GeV/c				
No. of parameters	6	7	8	9
$P(\chi^2)$	2.99×10^{-7}	1.09×10^{-2}	5.13×10^{-2}	4.51×10^{-2}
A_0	0.77 ± 0.04	1.01 ± 0.06	1.12 ± 0.07	1.08 ± 0.09
A_1	1.62 ± 0.12	2.23 ± 0.16	2.60 ± 0.21	2.49 ± 0.24
A_2	1.98 ± 0.15	2.95 ± 0.22	3.45 ± 0.29	3.26 ± 0.36
A_3	1.82 ± 0.15	2.77 ± 0.22	3.43 ± 0.33	3.23 ± 0.40
A_4	1.16 ± 0.10	2.17 ± 0.20	2.74 ± 0.29	2.48 ± 0.40
A_5	0.56 ± 0.08	1.13 ± 0.13	1.71 ± 0.25	1.52 ± 0.33
A_6		0.56 ± 0.10	0.85 ± 0.15	0.64 ± 0.27
A_7			0.28 ± 0.11	0.18 ± 0.15
A_8				-0.10 ± 0.11
A_9				
A_{10}				
σ_{el}	6.16 ± 0.34	8.09 ± 0.48	9.03 ± 0.60	8.70 ± 0.71
σ_{tot}	22.58 ± 0.87	28.75 ± 1.19	32.29 ± 1.64	30.88 ± 2.36

Table 20

LEGENDRE COEFFICIENTS OF K^-p ANGULAR DISTRIBUTIONS

1.884 GeV/c				
No. of parameters	6	7	8	9
$P(\chi^2)$	0.00	0.39	0.34	0.27
A_0	0.94 ± 0.04	1.19 ± 0.06	1.21 ± 0.07	1.20 ± 0.08
A_1	2.25 ± 0.13	2.61 ± 0.15	2.69 ± 0.19	2.67 ± 0.22
A_2	2.57 ± 0.15	3.63 ± 0.23	3.70 ± 0.26	3.66 ± 0.34
A_3	2.73 ± 0.19	3.36 ± 0.22	3.50 ± 0.32	3.47 ± 0.38
A_4	1.60 ± 0.11	2.83 ± 0.23	2.92 ± 0.28	2.87 ± 0.41
A_5	1.06 ± 0.11	1.46 ± 0.13	1.60 ± 0.27	1.57 ± 0.35
A_6		0.76 ± 0.13	0.81 ± 0.16	0.77 ± 0.31
A_7			0.08 ± 0.14	0.06 ± 0.18
A_8				-0.02 ± 0.14
A_9				
A_{10}				
σ_{el}	7.01 ± 0.33	8.91 ± 0.45	9.03 ± 0.50	8.98 ± 0.60
σ_{tot}	24.98 ± 0.76	29.80 ± 0.98	30.40 ± 1.42	30.17 ± 2.07

Table 21

LEGENDRE COEFFICIENTS OF K^-p ANGULAR DISTRIBUTIONS

1.934 GeV/c				
No. of parameters	7	8	9	10
$P(\chi^2)$	0.08	0.08	0.11	0.24
A_0	0.96 ± 0.05	1.02 ± 0.07	1.10 ± 0.09	1.19 ± 0.10
A_1	2.33 ± 0.15	2.50 ± 0.20	2.72 ± 0.25	3.00 ± 0.28
A_2	3.01 ± 0.20	3.24 ± 0.28	3.60 ± 0.36	4.01 ± 0.41
A_3	2.99 ± 0.21	3.28 ± 0.31	3.68 ± 0.41	4.22 ± 0.49
A_4	2.36 ± 0.18	2.61 ± 0.28	3.06 ± 0.40	3.62 ± 0.49
A_5	1.32 ± 0.12	1.57 ± 0.23	1.92 ± 0.33	2.51 ± 0.43
A_6	0.66 ± 0.08	0.79 ± 0.13	1.13 ± 0.25	1.61 ± 0.35
A_7		0.11 ± 0.09	0.29 ± 0.15	0.70 ± 0.25
A_8			0.14 ± 0.09	0.38 ± 0.15
A_9				0.18 ± 0.09
A_{10}				
σ_{el}	6.9 ± 0.4	7.4 ± 0.5	7.9 ± 0.6	8.6 ± 0.7
σ_{tot}	26.7 ± 0.9	28.1 ± 1.4	30.4 ± 1.9	33.5 ± 2.3

Table 22

LEGENDRE COEFFICIENTS OF K^-p ANGULAR DISTRIBUTIONS

1.984 GeV/c				
No. of parameters	8	9	10	11
$P(\chi^2)$	0.18	0.14	0.30	0.65
A_0	1.04 ± 0.06	1.02 ± 0.07	1.11 ± 0.08	1.21 ± 0.09
A_1	2.45 ± 0.16	2.40 ± 0.19	2.65 ± 0.22	2.99 ± 0.27
A_2	3.20 ± 0.22	3.12 ± 0.28	3.55 ± 0.34	4.00 ± 0.39
A_3	3.17 ± 0.26	3.07 ± 0.33	3.58 ± 0.41	4.27 ± 0.50
A_4	2.62 ± 0.23	2.51 ± 0.33	3.12 ± 0.44	3.83 ± 0.53
A_5	1.59 ± 0.20	1.50 ± 0.29	2.11 ± 0.41	2.93 ± 0.54
A_6	0.75 ± 0.13	0.66 ± 0.24	1.21 ± 0.35	2.02 ± 0.49
A_7	0.17 ± 0.09	0.12 ± 0.15	0.62 ± 0.28	1.29 ± 0.39
A_8		-0.04 ± 0.10	0.23 ± 0.16	0.88 ± 0.32
A_9			0.26 ± 0.12	0.57 ± 0.18
A_{10}				0.33 ± 0.14
σ_{el}	7.26 ± 0.39	7.14 ± 0.47	7.80 ± 0.56	8.46 ± 0.63
σ_{tot}	27.11 ± 1.15	26.56 ± 1.74	30.08 ± 2.19	34.54 ± 2.59

Table 23

LEGENDRE COEFFICIENTS OF K^-p ANGULAR DISTRIBUTIONS

2.034 GeV/c				
No. of parameters	8	9	10	11
$P(\chi^2)$	0.38	0.69	0.83	0.78
A_0	0.84 ± 0.07	0.93 ± 0.08	1.04 ± 0.10	1.05 ± 0.14
A_1	1.99 ± 0.17	2.38 ± 0.24	2.52 ± 0.26	2.52 ± 0.41
A_2	2.58 ± 0.26	3.03 ± 0.33	3.49 ± 0.42	3.50 ± 0.55
A_3	2.60 ± 0.27	3.27 ± 0.40	3.62 ± 0.45	3.62 ± 0.66
A_4	2.13 ± 0.26	2.75 ± 0.37	3.28 ± 0.49	3.29 ± 0.60
A_5	1.35 ± 0.21	1.90 ± 0.32	2.42 ± 0.44	2.41 ± 0.56
A_6	0.66 ± 0.12	1.17 ± 0.26	1.53 ± 0.33	1.52 ± 0.53
A_7	0.21 ± 0.09	0.44 ± 0.13	0.92 ± 0.31	0.92 ± 0.34
A_8		0.25 ± 0.11	0.37 ± 0.13	0.35 ± 0.43
A_9			0.25 ± 0.15	0.25 ± 0.15
A_{10}				0.01 ± 0.20
σ_{el}	5.7 ± 0.5	6.3 ± 0.5	7.1 ± 0.7	7.1 ± 0.7
σ_{tot}	23.9 ± 1.4	27.3 ± 1.8	29.9 ± 2.3	29.8 ± 2.8

Table 24

LEGENDRE COEFFICIENTS OF K^-p ANGULAR DISTRIBUTIONS

2.084 GeV/c				
No. of parameters	8	9	10	11
$P(\chi^2)$	0.60	0.54	0.71	0.69
A_0	1.01 ± 0.07	1.40 ± 0.09	1.13 ± 0.10	1.16 ± 0.11
A_1	2.43 ± 0.19	2.51 ± 0.25	2.77 ± 0.29	2.87 ± 0.32
A_2	3.23 ± 0.27	3.34 ± 0.37	3.76 ± 0.43	3.92 ± 0.48
A_3	3.27 ± 0.30	3.41 ± 0.41	3.92 ± 0.51	4.13 ± 0.57
A_4	2.86 ± 0.27	3.00 ± 0.40	3.55 ± 0.51	3.80 ± 0.59
A_5	1.85 ± 0.22	1.97 ± 0.33	2.52 ± 0.46	2.78 ± 0.56
A_6	0.98 ± 0.13	1.08 ± 0.25	1.55 ± 0.36	1.80 ± 0.48
A_7	0.43 ± 0.08	0.48 ± 0.15	0.86 ± 0.26	1.08 ± 0.37
A_8		0.04 ± 0.08	0.27 ± 0.15	0.45 ± 0.27
A_9			0.16 ± 0.09	0.27 ± 0.16
A_{10}				0.08 ± 0.09
σ_{el}	6.64 ± 0.46	6.81 ± 0.59	7.43 ± 0.68	7.65 ± 0.74
σ_{tot}	26.37 ± 1.24	27.02 ± 1.82	29.80 ± 2.23	31.10 ± 2.65

Table 25

LEGENDRE COEFFICIENTS OF K^-p ANGULAR DISTRIBUTIONS

2.134 GeV/c				
No. of parameters	7	8	9	10
$P(\chi^2)$	0.01	0.10	0.15	0.36
A_0	0.97 ± 0.06	1.21 ± 0.10	1.11 ± 0.11	1.93 ± 0.38
A_1	2.49 ± 0.18	2.58 ± 0.19	3.27 ± 0.45	1.89 ± 0.77
A_2	2.85 ± 0.21	3.70 ± 0.35	3.59 ± 0.36	6.16 ± 1.21
A_3	2.99 ± 0.25	3.53 ± 0.31	4.32 ± 0.55	3.76 ± 0.61
A_4	2.55 ± 0.22	3.19 ± 0.31	3.78 ± 0.46	4.69 ± 0.62
A_5	1.27 ± 0.13	2.19 ± 0.33	2.38 ± 0.35	4.50 ± 1.02
A_6	0.74 ± 0.14	0.90 ± 0.15	1.90 ± 0.60	0.82 ± 0.77
A_7		0.62 ± 0.21	0.50 ± 0.22	3.28 ± 1.27
A_8			0.57 ± 0.33	-0.32 ± 0.52
A_9				1.17 ± 0.53
A_{10}				
σ_{el}	6.2 ± 0.4	7.7 ± 0.7	7.1 ± 0.7	12.3 ± 2.5
σ_{tot}	23.8 ± 0.9	27.0 ± 1.3	29.6 ± 0.8	33.7 ± 2.4

Table 26

LEGENDRE COEFFICIENTS OF K^-p ANGULAR DISTRIBUTIONS

2.175 GeV/c				
No. of parameters	8	9	10	11
$P(\chi^2)$	0.13	0.10	0.21	0.47
A_0	1.15 ± 0.06	1.15 ± 0.08	1.27 ± 0.10	1.38 ± 0.11
A_1	2.69 ± 0.18	2.70 ± 0.22	3.03 ± 0.27	3.37 ± 0.31
A_2	3.57 ± 0.25	3.58 ± 0.33	4.07 ± 0.40	4.62 ± 0.47
A_3	3.69 ± 0.29	3.70 ± 0.37	4.40 ± 0.50	5.05 ± 0.58
A_4	3.23 ± 0.26	3.25 ± 0.39	3.94 ± 0.51	4.81 ± 0.64
A_5	1.98 ± 0.24	1.99 ± 0.33	3.79 ± 0.50	3.60 ± 0.62
A_6	1.00 ± 0.14	1.02 ± 0.28	1.67 ± 0.42	2.53 ± 0.57
A_7	0.25 ± 0.12	0.26 ± 0.17	0.85 ± 0.33	1.55 ± 0.46
A_8		0.01 ± 0.13	0.34 ± 0.20	0.98 ± 0.35
A_9			0.30 ± 0.15	0.61 ± 0.20
A_{10}				0.34 ± 0.16
σ_{el}	7.2 ± 0.4	7.2 ± 0.5	7.9 ± 0.6	8.61 ± 0.70
σ_{tot}	26.1 ± 1.1	26.2 ± 1.6	29.7 ± 2.1	33.5 ± 2.5

Table 27

LEGENDRE COEFFICIENTS OF K^-p ANGULAR DISTRIBUTIONS

2.284 GeV/c				
No. of parameters	8	9	10	11
$P(\chi^2)$	0.00	0.04	0.06	0.04
A_0	1.00 ± 0.06	1.16 ± 0.08	1.24 ± 0.09	1.27 ± 0.11
A_1	2.46 ± 0.17	2.86 ± 0.21	3.10 ± 0.26	3.19 ± 0.31
A_2	3.26 ± 0.24	3.96 ± 0.32	4.30 ± 0.39	4.46 ± 0.47
A_3	3.42 ± 0.28	4.16 ± 0.36	4.65 ± 0.48	4.83 ± 0.58
A_4	2.93 ± 0.25	3.85 ± 0.37	4.34 ± 0.49	4.56 ± 0.63
A_5	2.09 ± 0.23	2.84 ± 0.32	3.38 ± 0.47	3.59 ± 0.61
A_6	1.08 ± 0.14	1.84 ± 0.27	2.27 ± 0.38	2.49 ± 0.56
A_7	0.34 ± 0.11	0.74 ± 0.16	1.15 ± 0.31	1.33 ± 0.44
A_8		0.41 ± 0.13	0.63 ± 0.19	0.78 ± 0.34
A_9			0.20 ± 0.13	0.29 ± 0.20
A_{10}				0.07 ± 0.13
σ_{el}	5.9 ± 0.3	6.8 ± 0.5	7.3 ± 0.5	7.4 ± 0.6
σ_{tot}	23.9 ± 1.0	27.4 ± 1.3	29.5 ± 1.8	30.4 ± 2.4

Table 28

LEGENDRE COEFFICIENTS OF K^-p ANGULAR DISTRIBUTIONS

2.325 GeV/c				
No. of parameters	8	9	10	11
$P(\chi^2)$	0.00	0.13	0.40	0.34
A_0	0.83 ± 0.08	0.98 ± 0.10	1.12 ± 0.11	1.15 ± 0.12
A_1	1.98 ± 0.24	2.36 ± 0.28	2.86 ± 0.31	2.94 ± 0.33
A_2	2.70 ± 0.34	3.39 ± 0.41	4.06 ± 0.46	4.20 ± 0.50
A_3	2.79 ± 0.39	3.47 ± 0.45	4.52 ± 0.54	4.70 ± 0.60
A_4	2.51 ± 0.33	3.45 ± 0.46	4.46 ± 0.54	4.69 ± 0.64
A_5	1.71 ± 0.29	2.32 ± 0.36	3.58 ± 0.51	3.83 ± 0.63
A_6	0.82 ± 0.15	1.61 ± 0.31	2.53 ± 0.41	2.79 ± 0.56
A_7	0.31 ± 0.13	0.61 ± 0.17	1.57 ± 0.32	1.80 ± 0.46
A_8		0.38 ± 0.13	0.86 ± 0.19	1.06 ± 0.34
A_9			0.45 ± 0.13	0.56 ± 0.20
A_{10}				0.10 ± 0.14
σ_{el}	4.75 ± 0.50	5.62 ± 0.59	6.45 ± 0.63	6.61 ± 0.67
σ_{tot}	21.22 ± 1.47	24.75 ± 1.70	29.29 ± 1.87	30.29 ± 2.30

Table 29

LEGENDRE COEFFICIENTS OF K^-p ANGULAR DISTRIBUTIONS

2.374 GeV/c				
No. of parameters	8	9	10	11
$P(\chi^2)$	0.02	0.07	0.44	0.32
A_0	0.94 ± 0.09	1.06 ± 0.11	1.18 ± 0.12	1.18 ± 0.13
A_1	2.30 ± 0.27	2.59 ± 0.30	3.01 ± 0.34	3.03 ± 0.36
A_2	3.16 ± 0.37	3.71 ± 0.45	4.27 ± 0.49	4.29 ± 0.54
A_3	3.23 ± 0.41	3.81 ± 0.49	4.69 ± 0.59	4.71 ± 0.65
A_4	3.02 ± 0.36	3.73 ± 0.49	4.62 ± 0.59	4.65 ± 0.70
A_5	2.05 ± 0.30	2.63 ± 0.40	3.69 ± 0.56	3.72 ± 0.67
A_6	1.13 ± 0.19	1.73 ± 0.33	2.54 ± 0.45	2.57 ± 0.61
A_7	0.35 ± 0.13	0.67 ± 0.19	1.50 ± 0.36	1.53 ± 0.49
A_8		0.34 ± 0.16	0.78 ± 0.22	0.80 ± 0.36
A_9			0.39 ± 0.14	0.41 ± 0.23
A_{10}				0.01 ± 0.14
σ_{el}	5.26 ± 0.53	5.96 ± 0.62	6.62 ± 0.66	6.64 ± 0.70
σ_{tot}	22.52 ± 1.43	25.20 ± 1.24	28.90 ± 1.98	29.03 ± 2.46

Table 30

LEGENDRE COEFFICIENTS OF K^-p POLARIZATIONS

1.383 GeV/c				
No. of parameters	5	6	7	8
$P(X^2)$	0.03	0.13	0.11	0.10
B_1	0.15 ± 0.02	0.13 ± 0.02	0.16 ± 0.02	0.16 ± 0.02
B_2	0.22 ± 0.02	0.24 ± 0.03	0.24 ± 0.03	0.23 ± 0.03
B_3	0.19 ± 0.02	0.21 ± 0.02	0.21 ± 0.03	0.21 ± 0.03
B_4	0.04 ± 0.02	0.07 ± 0.02	0.07 ± 0.02	0.06 ± 0.03
B_5	-0.02 ± 0.02	0.00 ± 0.02	0.00 ± 0.02	-0.01 ± 0.03
B_6		0.04 ± 0.01	0.04 ± 0.02	0.02 ± 0.02
B_7			0.00 ± 0.01	-0.01 ± 0.02
B_8				-0.01 ± 0.01

Table 31

LEGENDRE COEFFICIENTS OF K^-p POLARIZATIONS

1.433 GeV/c				
No. of parameters	5	6	7	8
$P(\chi^2)$	0.80	0.82	0.78	0.72
B_1	0.12 ± 0.02	0.12 ± 0.02	0.12 ± 0.02	0.12 ± 0.02
B_2	0.22 ± 0.02	0.23 ± 0.02	0.23 ± 0.02	0.23 ± 0.02
B_3	0.18 ± 0.02	0.19 ± 0.02	0.18 ± 0.02	0.18 ± 0.02
B_4	0.05 ± 0.01	0.06 ± 0.02	0.06 ± 0.02	0.05 ± 0.02
B_5	-0.01 ± 0.01	0.00 ± 0.01	-0.01 ± 0.02	-0.01 ± 0.02
B_6		0.01 ± 0.01	0.01 ± 0.01	0.01 ± 0.02
B_7			0.00 ± 0.01	-0.01 ± 0.01
B_8				0.00 ± 0.01

Table 32

LEGENDRE COEFFICIENTS OF K^-p POLARIZATIONS

1.483 GeV/c				
No. of parameters	5	6	7	8
$P(\chi^2)$	0.28	0.71	0.67	0.69
B_1	0.09 ± 0.02	0.10 ± 0.02	0.10 ± 0.02	0.10 ± 0.02
B_2	0.17 ± 0.02	0.19 ± 0.02	0.19 ± 0.02	0.18 ± 0.02
B_3	0.17 ± 0.02	0.20 ± 0.02	0.19 ± 0.02	0.18 ± 0.02
B_4	0.02 ± 0.01	0.06 ± 0.02	0.05 ± 0.02	0.04 ± 0.02
B_5	-0.02 ± 0.01	-0.01 ± 0.01	-0.01 ± 0.02	-0.02 ± 0.02
B_6		0.03 ± 0.01	0.03 ± 0.01	0.01 ± 0.02
B_7			-0.01 ± 0.01	-0.01 ± 0.01
B_8				-0.01 ± 0.01

Table 33

LEGENDRE COEFFICIENTS OF K^-p POLARIZATIONS

1.534 GeV/c				
No. of parameters	5	6	7	8
$P(\chi^2)$	0.05	0.22	0.18	0.15
B_1	0.06 ± 0.02	0.08 ± 0.02	0.07 ± 0.02	0.08 ± 0.02
B_2	0.14 ± 0.02	0.17 ± 0.02	0.16 ± 0.02	0.17 ± 0.02
B_3	0.14 ± 0.02	0.16 ± 0.02	0.16 ± 0.02	0.16 ± 0.02
B_4	0.02 ± 0.02	0.05 ± 0.02	0.05 ± 0.02	0.06 ± 0.02
B_5	-0.01 ± 0.01	0.00 ± 0.01	0.00 ± 0.02	0.01 ± 0.02
B_6		0.03 ± 0.01	0.03 ± 0.01	0.04 ± 0.02
B_7			0.00 ± 0.01	0.00 ± 0.01
B_8				0.01 ± 0.01

Table 34

LEGENDRE COEFFICIENTS OF K^-p POLARIZATIONS

1.584 GeV/c				
No. of parameters	5	6	7	8
$P(\chi^2)$	0.01	0.04	0.08	0.07
B_1	0.05 ± 0.02	0.06 ± 0.02	0.05 ± 0.02	0.06 ± 0.02
B_2	0.15 ± 0.02	0.17 ± 0.02	0.16 ± 0.02	0.17 ± 0.02
B_3	0.13 ± 0.02	0.15 ± 0.02	0.13 ± 0.02	0.14 ± 0.03
B_4	0.05 ± 0.01	0.08 ± 0.02	0.06 ± 0.02	0.07 ± 0.03
B_5	0.01 ± 0.01	0.02 ± 0.01	0.00 ± 0.02	0.00 ± 0.02
B_6		0.03 ± 0.01	0.02 ± 0.01	0.03 ± 0.02
B_7			-0.02 ± 0.01	-0.02 ± 0.01
B_8				0.01 ± 0.01

Table 35

LEGENDRE COEFFICIENTS OF K^-p POLARIZATIONS

1.634 GeV/c				
No. of parameters	5	6	7	8
$P(\chi^2)$	0.80	0.77	0.82	0.84
B_1	0.02 ± 0.02	0.02 ± 0.03	0.01 ± 0.03	0.02 ± 0.03
B_2	0.16 ± 0.03	0.17 ± 0.03	0.16 ± 0.03	0.18 ± 0.03
B_3	0.13 ± 0.03	0.14 ± 0.03	0.11 ± 0.03	0.12 ± 0.04
B_4	0.02 ± 0.02	0.03 ± 0.03	0.01 ± 0.03	0.04 ± 0.04
B_5	0.01 ± 0.02	0.01 ± 0.02	-0.02 ± 0.03	-0.01 ± 0.03
B_6		0.01 ± 0.02	0.00 ± 0.02	0.02 ± 0.03
B_7			-0.02 ± 0.02	-0.01 ± 0.02
B_8				0.02 ± 0.02

Table 36

LEGENDRE COEFFICIENTS OF K^-p POLARIZATIONS

1.684 GeV/c				
No. of parameters	5	6	7	8
$P(\chi^2)$	0.06	0.51	0.90	0.89
B_1	0.03 ± 0.02	0.05 ± 0.02	0.06 ± 0.02	0.07 ± 0.02
B_2	0.15 ± 0.02	0.19 ± 0.03	0.21 ± 0.03	0.22 ± 0.03
B_3	0.15 ± 0.02	0.19 ± 0.02	0.22 ± 0.03	0.23 ± 0.03
B_4	0.05 ± 0.02	0.11 ± 0.02	0.14 ± 0.03	0.15 ± 0.03
B_5	0.02 ± 0.01	0.05 ± 0.02	0.09 ± 0.02	0.10 ± 0.03
B_6		0.05 ± 0.01	0.07 ± 0.02	0.08 ± 0.02
B_7			0.04 ± 0.01	0.04 ± 0.02
B_8				0.01 ± 0.01

Table 37

LEGENDRE COEFFICIENTS OF K^-p POLARIZATIONS

1.734 GeV/c				
No. of parameters	5	6	7	8
$P(\chi^2)$	0.09	0.77	0.73	0.71
B_1	0.02 ± 0.02	0.04 ± 0.02	0.04 ± 0.02	0.04 ± 0.02
B_2	0.16 ± 0.02	0.21 ± 0.02	0.20 ± 0.03	0.21 ± 0.03
B_3	0.19 ± 0.02	0.22 ± 0.02	0.22 ± 0.03	0.23 ± 0.03
B_4	0.09 ± 0.02	0.14 ± 0.02	0.14 ± 0.02	0.15 ± 0.03
B_5	0.03 ± 0.01	0.06 ± 0.02	0.05 ± 0.02	0.06 ± 0.03
B_6		0.05 ± 0.01	0.04 ± 0.01	0.06 ± 0.02
B_7			-0.01 ± 0.01	0.00 ± 0.02
B_8				0.01 ± 0.01

Table 38

LEGENDRE COEFFICIENTS OF K^-p POLARIZATIONS

1.784 GeV/c				
No. of parameters	5	6	7	8
$P(\chi^2)$	0.16	0.15	0.34	0.28
B_1	-0.01 ± 0.02	-0.01 ± 0.02	-0.02 ± 0.02	-0.02 ± 0.02
B_2	0.13 ± 0.02	0.13 ± 0.02	0.12 ± 0.02	0.12 ± 0.03
B_3	0.11 ± 0.02	0.12 ± 0.02	0.09 ± 0.03	0.09 ± 0.03
B_4	0.05 ± 0.01	0.06 ± 0.02	0.04 ± 0.02	0.04 ± 0.03
B_5	0.02 ± 0.01	0.03 ± 0.01	-0.01 ± 0.02	-0.01 ± 0.02
B_6		0.01 ± 0.01	-0.01 ± 0.01	-0.01 ± 0.02
B_7			-0.03 ± 0.01	-0.03 ± 0.01
B_8				0.00 ± 0.01

Table 39

LEGENDRE COEFFICIENTS OF K^-p POLARIZATIONS

1.884 GeV/c				
No. of parameters	5	6	7	8
$P(\chi^2)$	0.66	0.59	0.55	0.48
B_1	0.08 ± 0.02	0.08 ± 0.03	0.09 ± 0.03	0.09 ± 0.03
B_2	0.20 ± 0.03	0.20 ± 0.03	0.20 ± 0.03	0.21 ± 0.04
B_3	0.20 ± 0.03	0.20 ± 0.03	0.22 ± 0.04	0.22 ± 0.04
B_4	0.08 ± 0.02	0.08 ± 0.03	0.09 ± 0.03	0.10 ± 0.04
B_5	0.06 ± 0.02	0.06 ± 0.02	0.07 ± 0.03	0.08 ± 0.03
B_6		0.00 ± 0.02	0.00 ± 0.02	0.01 ± 0.03
B_7			0.01 ± 0.02	0.01 ± 0.02
B_8				0.01 ± 0.02

Table 40

LEGENDRE COEFFICIENTS OF K^-p POLARIZATIONS

1.934 GeV/c				
No. of parameters	6	7	8	9
$P(\chi^2)$	0.39	0.62	0.71	0.74
B_1	0.10 ± 0.02	0.10 ± 0.02	0.11 ± 0.02	0.11 ± 0.02
B_2	0.17 ± 0.02	0.18 ± 0.02	0.19 ± 0.02	0.19 ± 0.02
B_3	0.17 ± 0.02	0.19 ± 0.02	0.20 ± 0.02	0.20 ± 0.02
B_4	0.12 ± 0.01	0.14 ± 0.02	0.15 ± 0.02	0.16 ± 0.02
B_5	0.06 ± 0.01	0.08 ± 0.01	0.09 ± 0.02	0.11 ± 0.02
B_6	0.03 ± 0.01	0.04 ± 0.01	0.05 ± 0.02	0.06 ± 0.02
B_7		0.02 ± 0.01	0.02 ± 0.01	0.04 ± 0.02
B_8			0.01 ± 0.01	0.02 ± 0.01
B_9				0.01 ± 0.01

Table 41

LEGENDRE COEFFICIENTS OF K^-p POLARIZATIONS

1.984 GeV/c				
No. of parameters	6	7	8	9
$P(\chi^2)$	0.58	0.56	0.53	0.49
B_1	0.05 ± 0.02	0.06 ± 0.02	0.06 ± 0.02	0.06 ± 0.02
B_2	0.14 ± 0.02	0.15 ± 0.02	0.16 ± 0.03	0.16 ± 0.03
B_3	0.16 ± 0.02	0.18 ± 0.03	0.18 ± 0.03	0.19 ± 0.03
B_4	0.07 ± 0.02	0.08 ± 0.02	0.10 ± 0.03	0.10 ± 0.03
B_5	0.04 ± 0.01	0.06 ± 0.02	0.06 ± 0.02	0.08 ± 0.04
B_6	0.00 ± 0.01	0.00 ± 0.01	0.02 ± 0.03	0.02 ± 0.03
B_7		0.01 ± 0.01	0.01 ± 0.01	0.03 ± 0.03
B_8			0.01 ± 0.01	0.01 ± 0.01
B_9				0.01 ± 0.01

Table 42

LEGENDRE COEFFICIENTS OF K^-p POLARIZATIONS

2.034 GeV/c				
No. of parameters	6	7	8	9
$P(\chi^2)$	0.16	0.55	0.54	0.47
B_1	0.06 ± 0.01	0.09 ± 0.02	0.08 ± 0.02	0.08 ± 0.02
B_2	0.18 ± 0.02	0.16 ± 0.02	0.17 ± 0.02	0.17 ± 0.03
B_3	0.12 ± 0.02	0.17 ± 0.03	0.17 ± 0.03	0.17 ± 0.03
B_4	0.13 ± 0.02	0.12 ± 0.02	0.13 ± 0.03	0.13 ± 0.03
B_5	0.04 ± 0.01	0.09 ± 0.02	0.09 ± 0.02	0.09 ± 0.02
B_6	0.04 ± 0.01	0.03 ± 0.01	0.04 ± 0.02	0.04 ± 0.02
B_7		0.03 ± 0.01	0.03 ± 0.01	0.03 ± 0.02
B_8			0.01 ± 0.01	0.01 ± 0.01
B_9				0.00 ± 0.01

Table 43

LEGENDRE COEFFICIENTS OF K^-p POLARIZATIONS

2.084 GeV/c				
No. of parameters	6	7	8	9
$P(\chi^2)$	0.12	0.30	0.46	0.41
B_1	0.10 ± 0.02	0.11 ± 0.02	0.12 ± 0.02	0.12 ± 0.02
B_2	0.16 ± 0.02	0.18 ± 0.02	0.19 ± 0.02	0.19 ± 0.02
B_3	0.18 ± 0.02	0.21 ± 0.02	0.22 ± 0.02	0.23 ± 0.03
B_4	0.09 ± 0.02	0.12 ± 0.02	0.14 ± 0.02	0.15 ± 0.03
B_5	0.06 ± 0.01	0.09 ± 0.02	0.11 ± 0.02	0.12 ± 0.02
B_6	0.01 ± 0.01	0.02 ± 0.01	0.05 ± 0.02	0.06 ± 0.02
B_7		0.02 ± 0.01	0.03 ± 0.01	0.04 ± 0.02
B_8			0.02 ± 0.01	0.02 ± 0.01
B_9				0.01 ± 0.01

Table 44

LEGENDRE COEFFICIENTS OF K^-p POLARIZATIONS

2.134 GeV/c				
No. of parameters	5	6	7	8
$P(\chi^2)$	0.63	0.63	0.68	0.82
B_1	0.09 ± 0.05	0.09 ± 0.05	0.15 ± 0.07	0.17 ± 0.07
B_2	0.22 ± 0.08	0.17 ± 0.06	0.17 ± 0.09	0.18 ± 0.09
B_3	0.21 ± 0.07	0.20 ± 0.07	0.29 ± 0.10	0.32 ± 0.10
B_4	0.17 ± 0.07	0.16 ± 0.07	0.12 ± 0.08	0.16 ± 0.08
B_5	0.04 ± 0.04	0.04 ± 0.03	0.11 ± 0.06	0.12 ± 0.06
B_6	0.04 ± 0.03	0.03 ± 0.03	0.02 ± 0.03	0.07 ± 0.05
B_7			0.03 ± 0.02	0.03 ± 0.02
B_8				0.03 ± 0.02

Table 45

LEGENDRE COEFFICIENTS OF K^-p POLARIZATIONS

2.175 GeV/c				
No. of parameters	6	7	8	9
$P(\chi^2)$	0.56	0.55	0.53	0.47
B_1	0.08 ± 0.02	0.09 ± 0.02	0.09 ± 0.02	0.09 ± 0.03
B_2	0.20 ± 0.03	0.20 ± 0.03	0.21 ± 0.03	0.21 ± 0.03
B_3	0.20 ± 0.02	0.21 ± 0.03	0.22 ± 0.03	0.22 ± 0.03
B_4	0.12 ± 0.02	0.13 ± 0.03	0.14 ± 0.03	0.14 ± 0.03
B_5	0.05 ± 0.02	0.07 ± 0.02	0.08 ± 0.03	0.08 ± 0.03
B_6	0.02 ± 0.01	0.02 ± 0.02	0.04 ± 0.02	0.04 ± 0.02
B_7		0.01 ± 0.01	0.02 ± 0.01	0.03 ± 0.02
B_8			0.01 ± 0.01	0.01 ± 0.01
B_9				0.01 ± 0.01

Table 46

LEGENDRE COEFFICIENTS OF K^- POLARIZATIONS

2.284 GeV/c				
No. of parameters	6	7	8	9
$P(\chi^2)$	0.07	0.18	0.14	0.23
B_1	0.07 ± 0.02	0.08 ± 0.02	0.09 ± 0.02	0.07 ± 0.02
B_2	0.15 ± 0.02	0.17 ± 0.02	0.18 ± 0.03	0.17 ± 0.03
B_3	0.16 ± 0.02	0.19 ± 0.03	0.20 ± 0.03	0.17 ± 0.03
B_4	0.11 ± 0.02	0.14 ± 0.02	0.15 ± 0.03	0.13 ± 0.03
B_5	0.06 ± 0.02	0.09 ± 0.02	0.10 ± 0.02	0.07 ± 0.03
B_6	0.01 ± 0.01	0.03 ± 0.01	0.04 ± 0.02	0.02 ± 0.02
B_7		0.03 ± 0.01	0.03 ± 0.01	0.00 ± 0.02
B_8			0.01 ± 0.01	-0.01 ± 0.01
B_9				-0.02 ± 0.01

Table 47

LEGENDRE COEFFICIENTS OF K^-p POLARIZATIONS

2.325 GeV/c				
No. of parameters	6	7	8	9
$P(\chi^2)$	0.11	0.82	0.74	0.75
B_1	0.06 ± 0.02	0.08 ± 0.02	0.08 ± 0.02	0.08 ± 0.02
B_2	0.14 ± 0.02	0.17 ± 0.02	0.17 ± 0.03	0.18 ± 0.03
B_3	0.17 ± 0.02	0.21 ± 0.03	0.21 ± 0.03	0.22 ± 0.03
B_4	0.13 ± 0.02	0.17 ± 0.02	0.17 ± 0.03	0.18 ± 0.03
B_5	0.06 ± 0.02	0.11 ± 0.02	0.11 ± 0.02	0.12 ± 0.03
B_6	0.04 ± 0.01	0.06 ± 0.01	0.06 ± 0.02	0.06 ± 0.02
B_7		0.04 ± 0.01	0.04 ± 0.01	0.06 ± 0.02
B_8			0.00 ± 0.01	0.00 ± 0.01
B_9				0.01 ± 0.01

Table 48

LEGENDRE COEFFICIENTS OF K^-p POLARIZATIONS

2.374 GeV/c				
No. of parameters	6	7	8	9
$P(\chi^2)$	0.03	0.11	0.89	0.90
B_1	0.10 ± 0.02	0.12 ± 0.02	0.13 ± 0.02	0.12 ± 0.03
B_2	0.15 ± 0.02	0.17 ± 0.03	0.21 ± 0.03	0.20 ± 0.03
B_3	0.17 ± 0.02	0.20 ± 0.03	0.24 ± 0.03	0.22 ± 0.03
B_4	0.14 ± 0.02	0.16 ± 0.02	0.21 ± 0.03	0.20 ± 0.03
B_5	0.07 ± 0.02	0.11 ± 0.02	0.15 ± 0.03	0.13 ± 0.03
B_6	0.04 ± 0.01	0.06 ± 0.02	0.11 ± 0.02	0.09 ± 0.03
B_7		0.03 ± 0.01	0.06 ± 0.02	0.05 ± 0.02
B_8			0.04 ± 0.01	0.03 ± 0.02
B_9				-0.01 ± 0.02

Figure captions

Fig. 1 : Layout of the apparatus. The beam enters from the right-hand side, traverses the beam telescope counters and interacts in the LMN target positioned in the middle of the magnet. The scattered kaon and the recoil proton traverse the counter hodoscope placed on a circle with a radius of 56 cm around the target.

Fig. 2 : Correlation histograms of left-hand counter No. 4 as a function of the right-hand counters for the five possible differences in the azimuthal angle. The incident beam momentum is 1.63 GeV/c. The dots represent the same spectra obtained with a dummy target. At $\cos \vartheta_{c.m.} = 0.76$ the differential cross-section is ~ 1.4 mb/sr, at $\cos \vartheta_{c.m.} = -0.8$ it is ~ 0.2 mb/sr.

Fig. 3 : Illustration of the background subtraction procedure as applied to the data of Fig. 2. The full line shows the sum of the two upper spectra of Fig. 2, containing the elastic peak, the dots show the same sum obtained from the dummy target data, while the dotted line represents the background spectrum as derived from the non-coplanar events of the polarized target run (the full lines of the lower three diagrams of Fig. 2).

Fig. 4 : A comparison between experimental (full line) and Monte Carlo (dotted line) angular correlations. Incident kaon momentum 1.48 GeV/c, left-hand counter No. 6.

Fig. 5 : Location of the elastic peaks in the plane formed by the left- and right-hand counters. The limits of the angular ranges used in this experiment are indicated by their centre-of-mass scattering angles. The incident momentum is 1.48 GeV/c.

Fig. 6 : Angular distributions and polarizations obtained at 1.38, 1.43 and 1.48 GeV/c incident momentum. The open circles in the differential cross-section diagrams represent the points deduced from literature data as discussed in the text. The lines represent the Legendre fits to the data. The fit to P is obtained by dividing the fit to $P(d\sigma/d\Omega)$ by the fit to the angular distribution. The vertical scale has an uncertainty of ±8%.

Fig. 7 : Angular distributions and polarizations obtained at 1.53, 1.58, and 1.63 GeV/c incident kaon momentum. For further explanation, see the caption of Fig. 6.

Fig. 8 : Angular distributions and polarizations obtained at 1.68, 1.73 and 1.78 GeV/c incident kaon momentum.

Fig. 9 : Angular distributions and polarizations obtained at 1.88, 1.93 and 1.98 GeV/c incident kaon momentum.

Fig.10 : Angular distributions and polarizations obtained at 2.03, 2.08 and 2.13 GeV/c incident kaon momentum.

Fig.11 : Angular distributions and polarizations obtained at 2.18, 2.28 and 2.33 GeV/c incident kaon momentum.

Fig.12 : Total cross-sections and total elastic cross-sections for K^-p scattering below 2.6 GeV/c. The total cross-sections are taken from Cool et al.[2]. Reference 6 lists the publications from which the elastic cross-sections are taken. The numbers and the arrows indicate the masses and the corresponding incident K^- momenta of the known Y^* resonances.

Fig.13 : Plots of the coefficients A_ℓ of the Legendre expansion of the differential cross-sections.

Fig.14 : The coefficients B_ℓ obtained from the Legendre expansion of $P(d\sigma/d\Omega)$. The open circles are points from Ref. 7.

Fig.15 : Polarization at $\cos \vartheta_{c.m.} = 0$ as obtained from the Legendre fits.

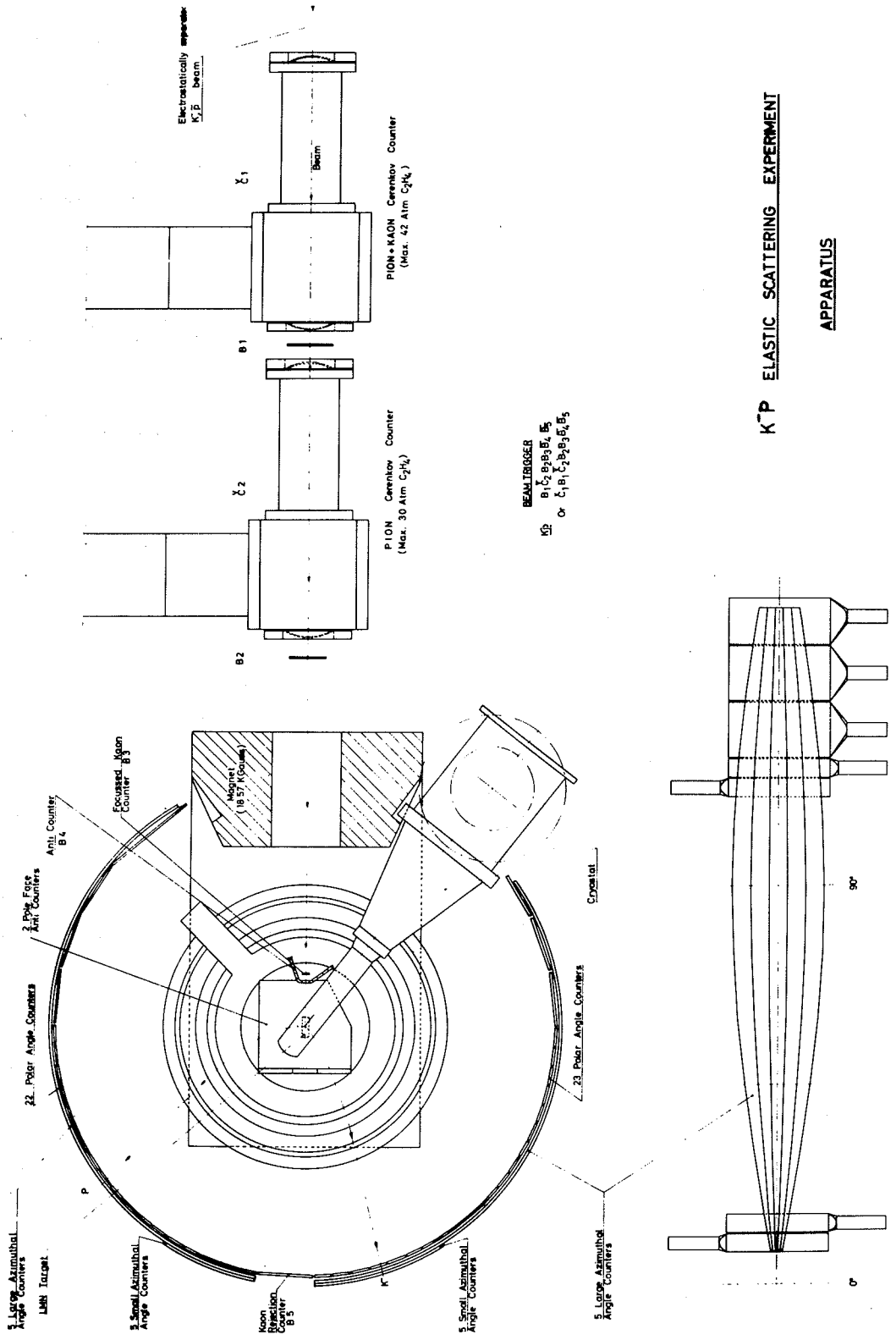
K⁻P ELASTIC SCATTERING EXPERMENT
APPARATUS
Electrostatically separated K⁻,p beam
Beam
PION • KAON Cerenkov Counter (Max. 42 Atm C_2H_6)
PION Cerenkov Counter (Max. 30 Atm C_2H_6)
BEAM TRIGGER
$B_1\bar{C}_2B_2B_3B_4B_5$
Or $\bar{C}_1B_1\bar{C}_2B_2B_3B_4B_5$
Focussed Kaon Counter B3
Anti Counter B4
2 Pole Face Anti Counters
Magnet (18.57 KGauss)
22 Polar Angle Counters
23 Polar Angle Counters
Crystal
5 Large Azimuthal Angle Counters
LMN Target
5 Small Azimuthal Angle Counters
Kaon Rejection Counter B5
90°
0°

Fig. 1

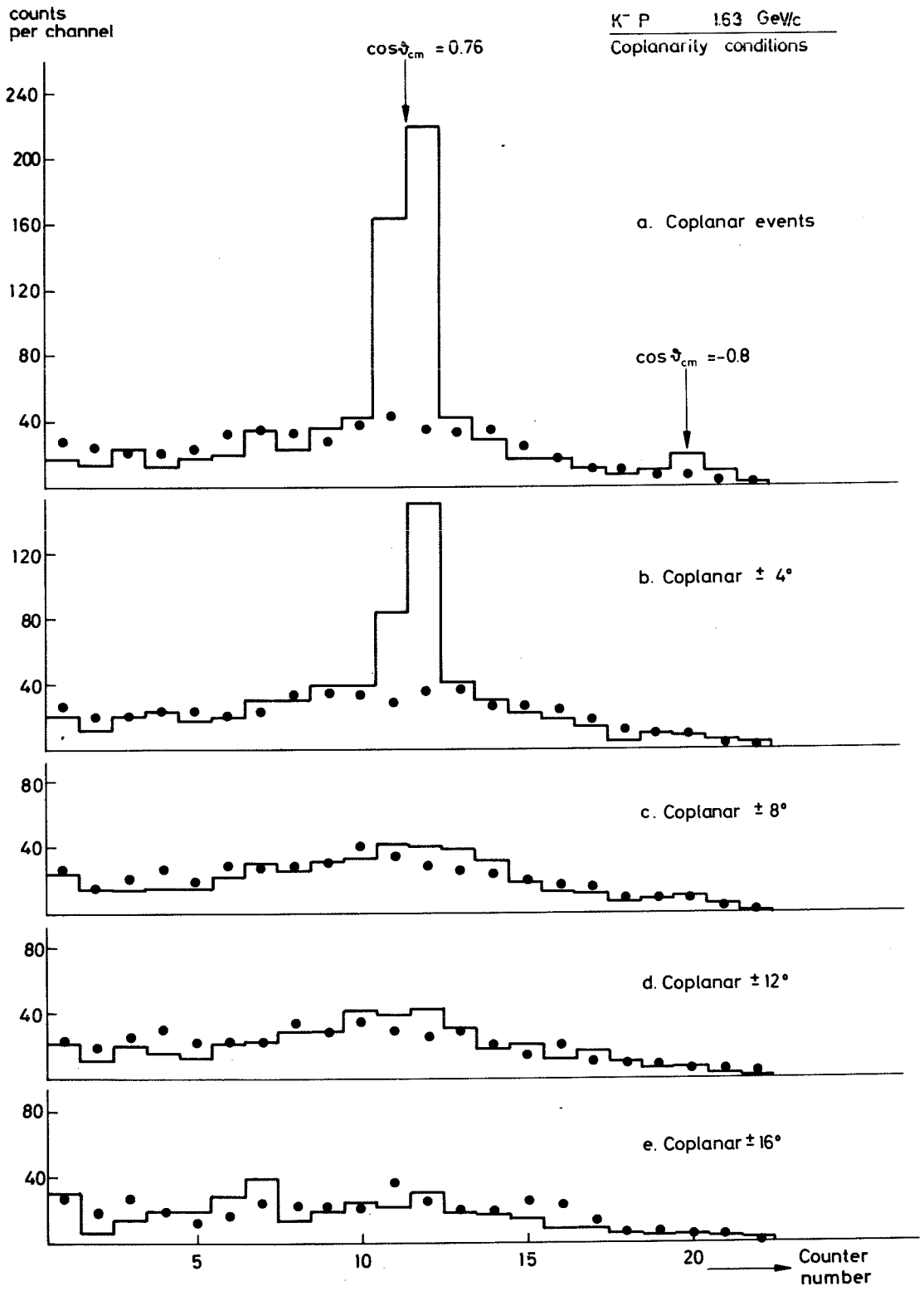

Fig. 2

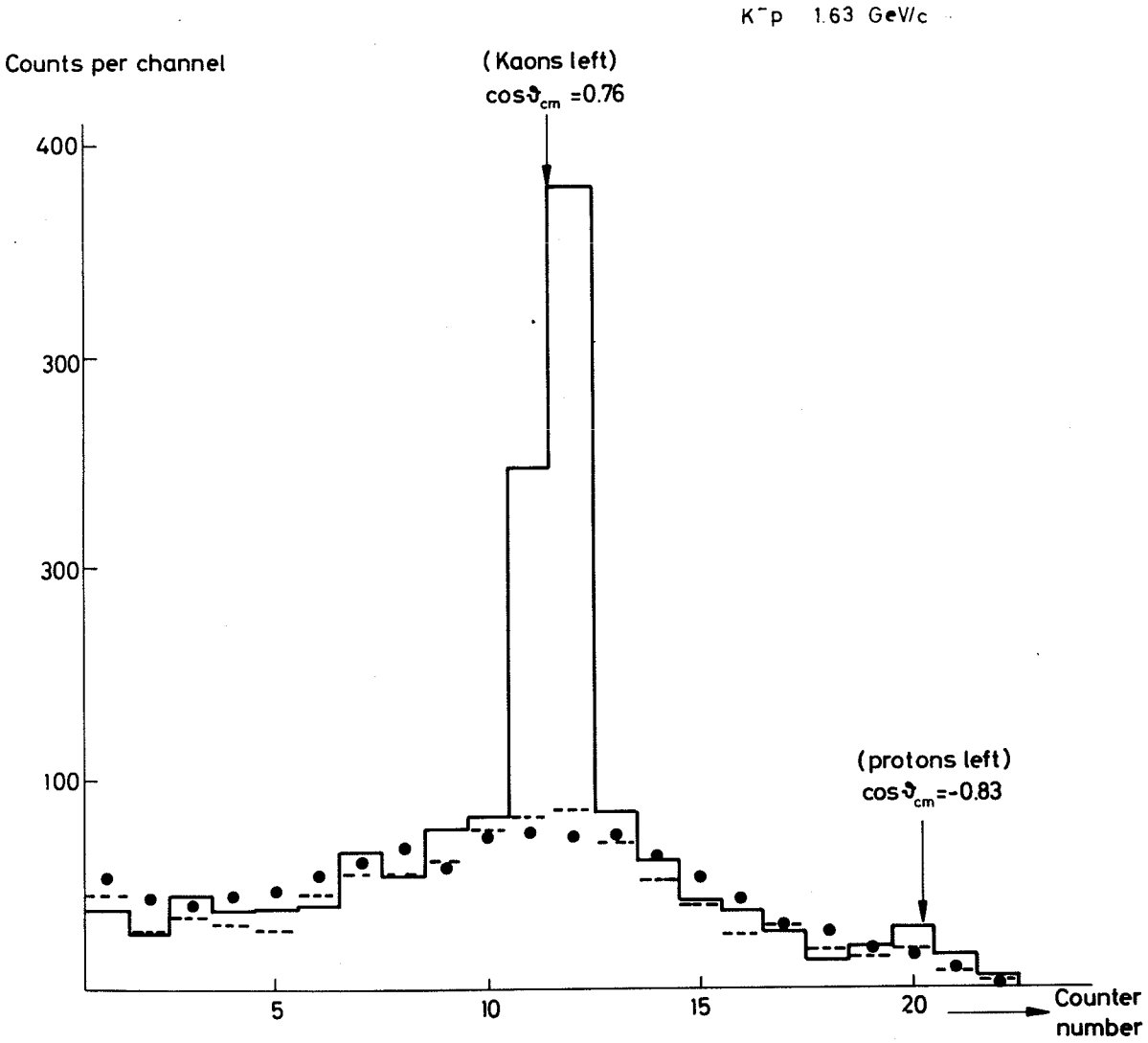
K⁻p 1.63 GeV/c
Counts per channel
(Kaons left)
cosϑ_{cm} =0.76
400
300
300
100
(protons left)
cosϑ_{cm}=-0.83
5
10
15
20
Counter number

Fig. 3

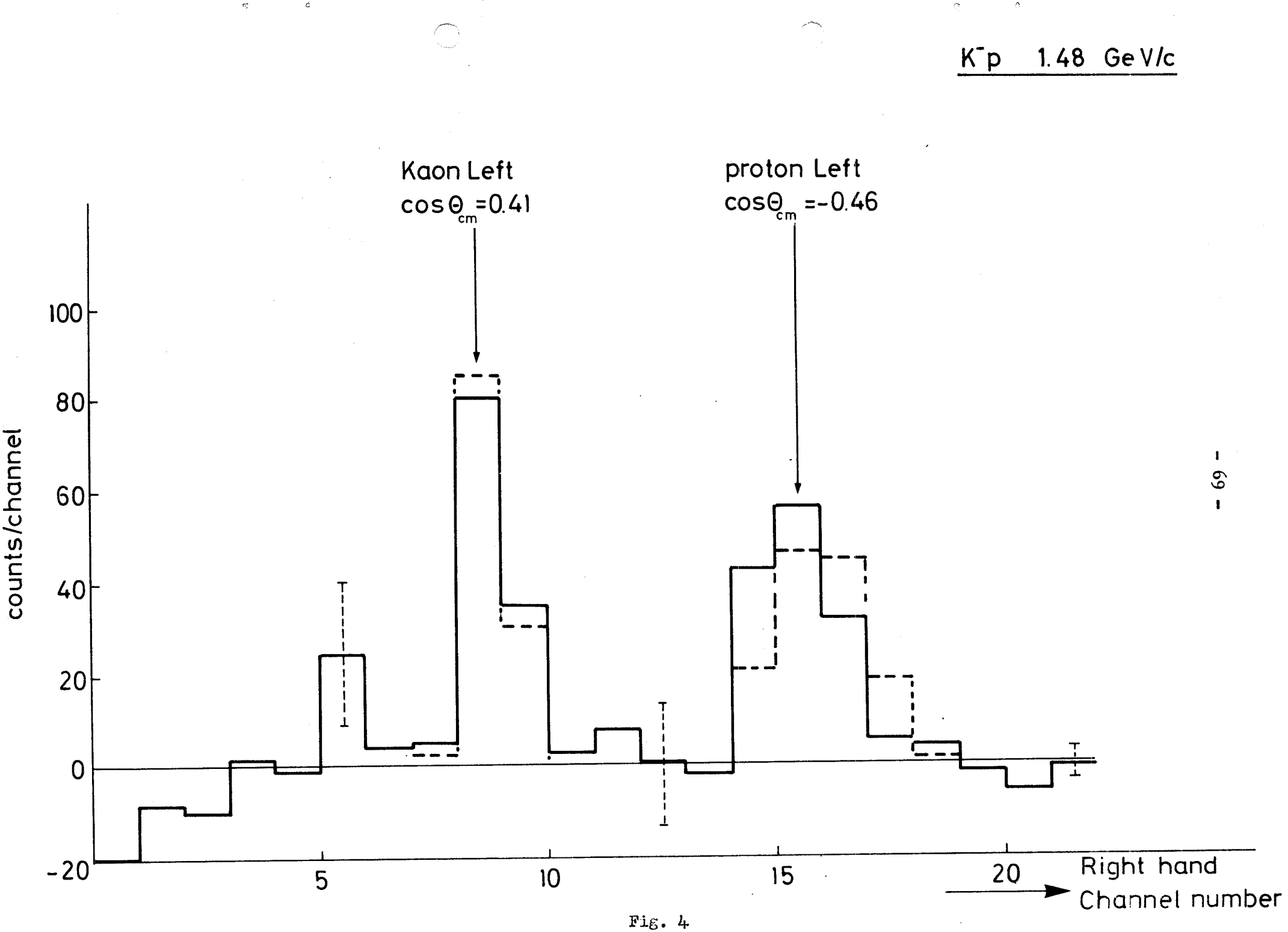
K⁻p 1.48 GeV/c
Kaon Left
cos Θcm =0.41
proton Left
cos Θcm =-0.46
counts/channel
100
80
60
40
20
0
-20
5
10
15
20
Right hand
Channel number

Fig. 4

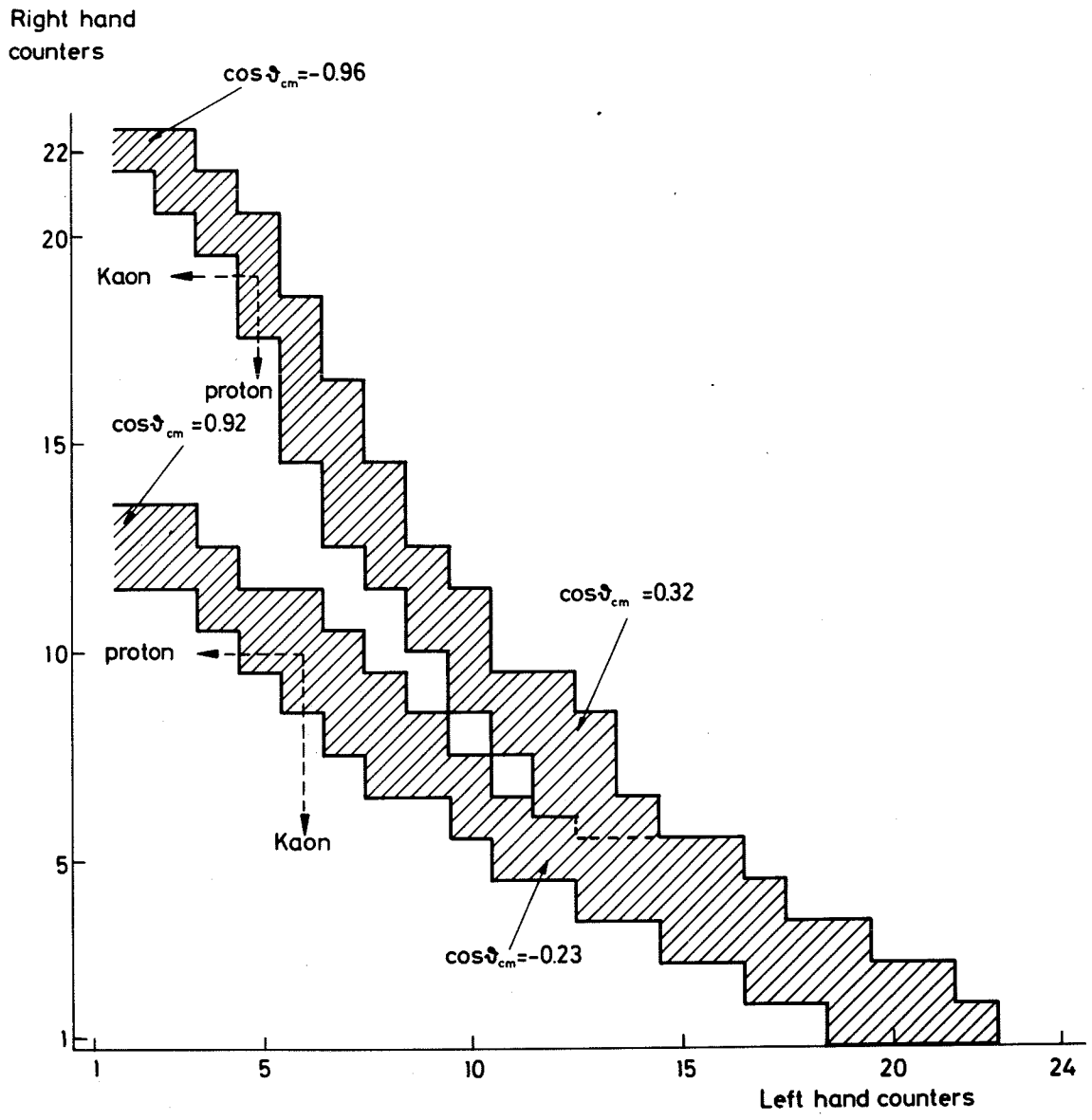
Right hand
counters
cosϑ_{cm}=-0.96
Kaon
proton
cosϑ_{cm} =0.92
cosϑ_{cm} =0.32
proton
Kaon
cosϑ_{cm}=-0.23
22
20
15
10
5
1
1
5
10
15
20
24
Left hand counters

Fig. 5

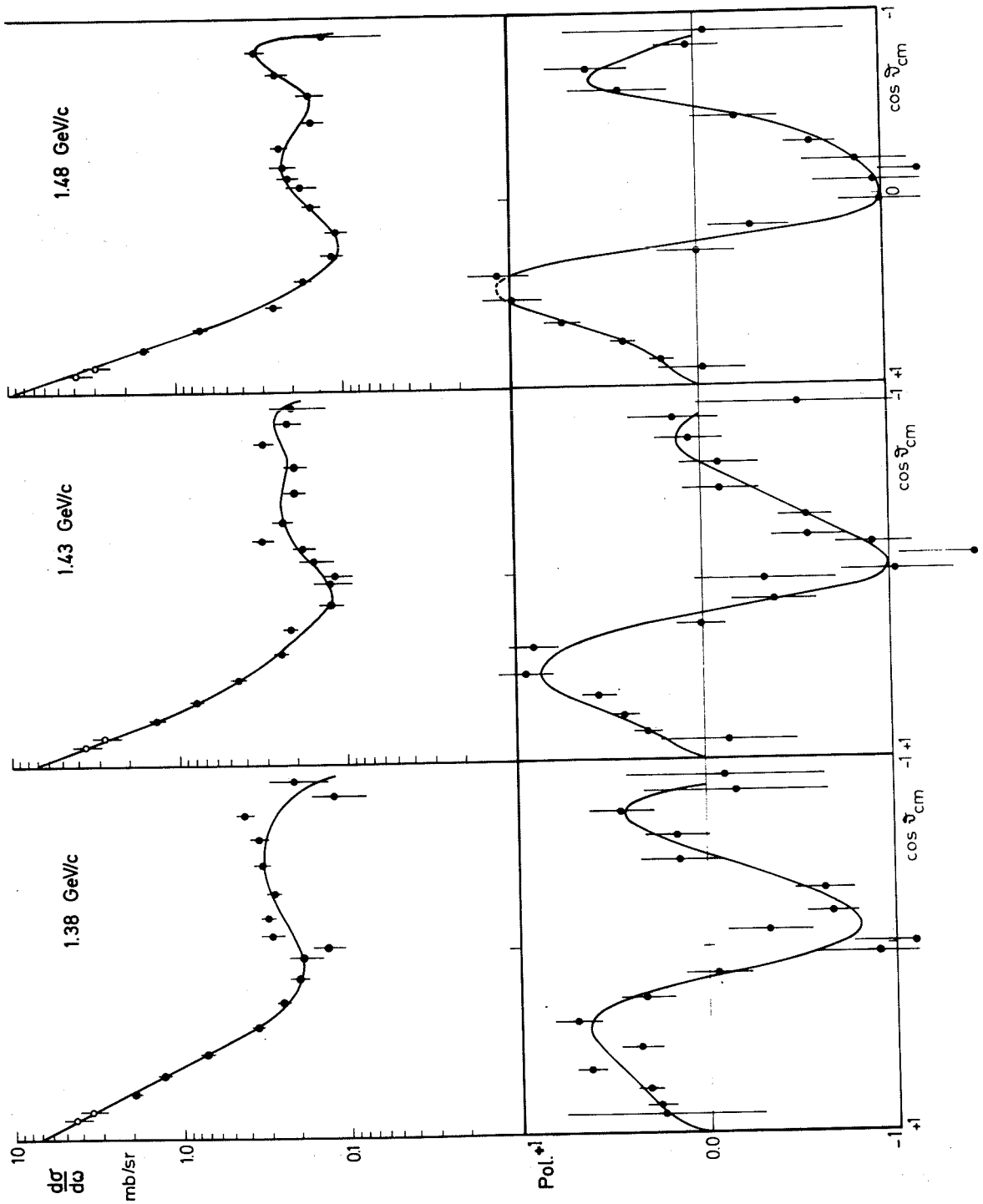

Fig. 6

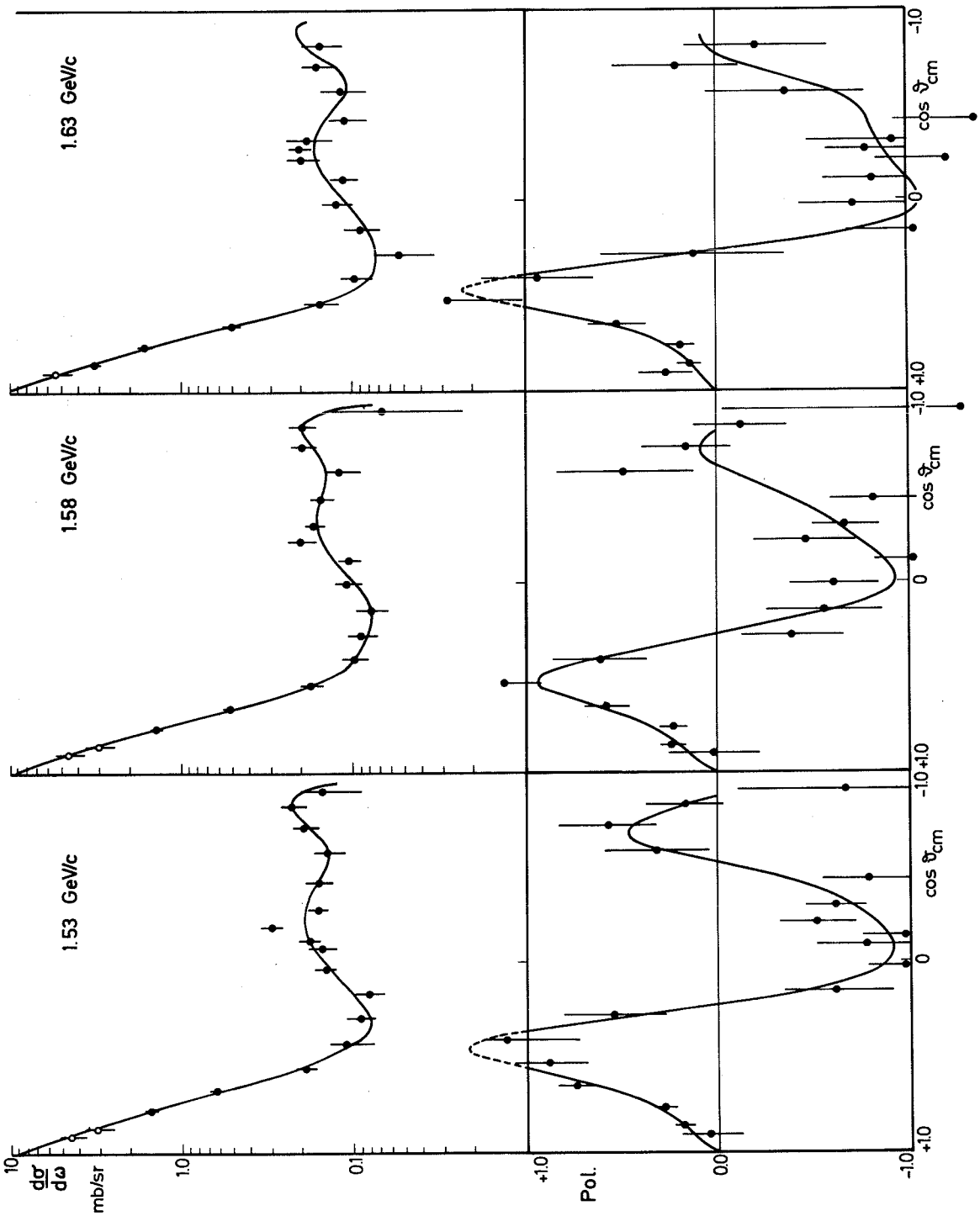
1.63 GeV/c
1.58 GeV/c
1.53 GeV/c
dσ/dω
mb/sr
10
1.0
0.1
Pol.
+1.0
0.0
-1.0
cos ϑcm
-1.0
0
+1.0

Fig. 7

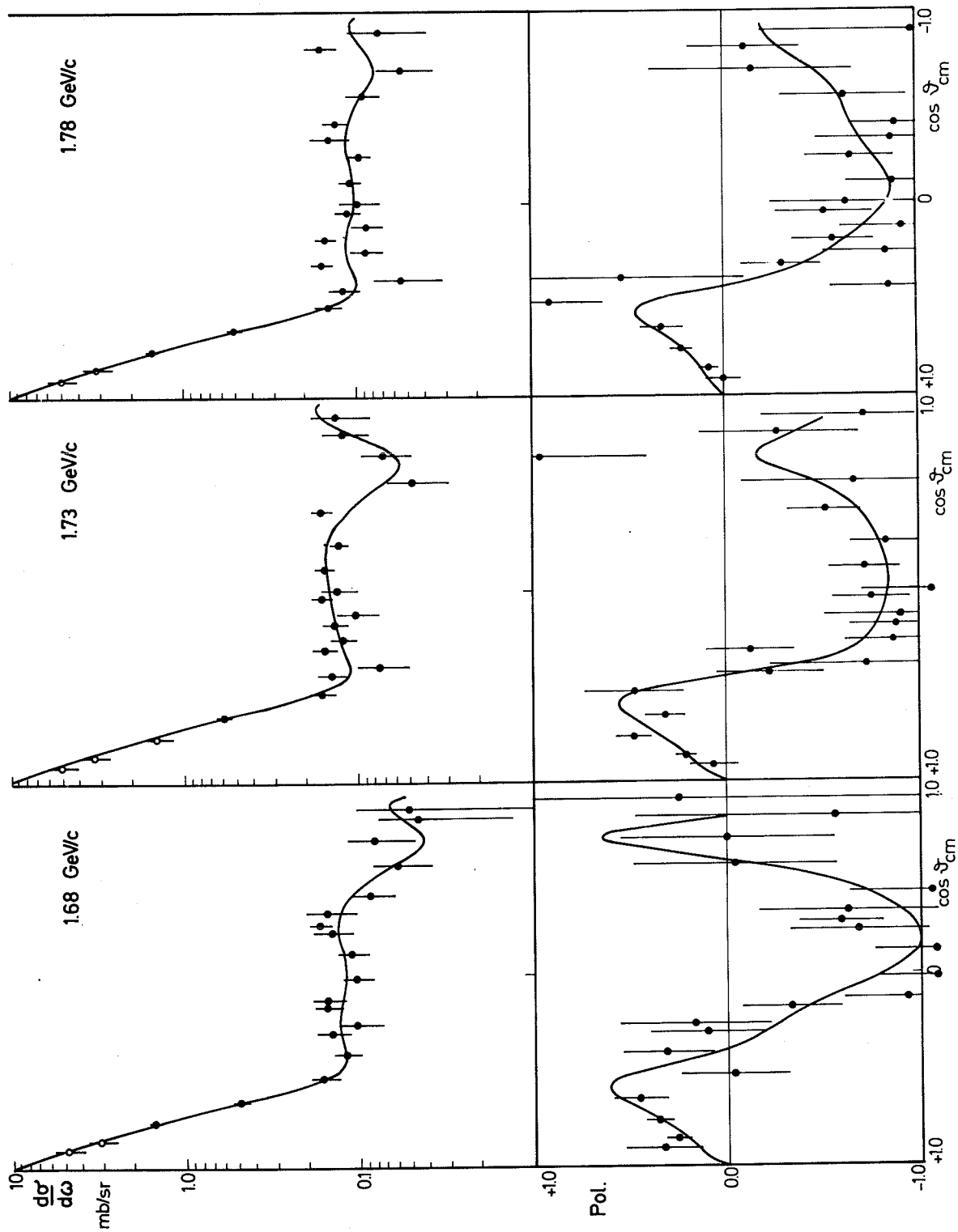
1.78 GeV/c
1.73 GeV/c
1.68 GeV/c
dσ/dΩ
mb/sr
10
1.0
0.1
Pol.
+1.0
0.0
-1.0
cos ϑcm
-1.0
0
1.0 +1.0

Fig. 8

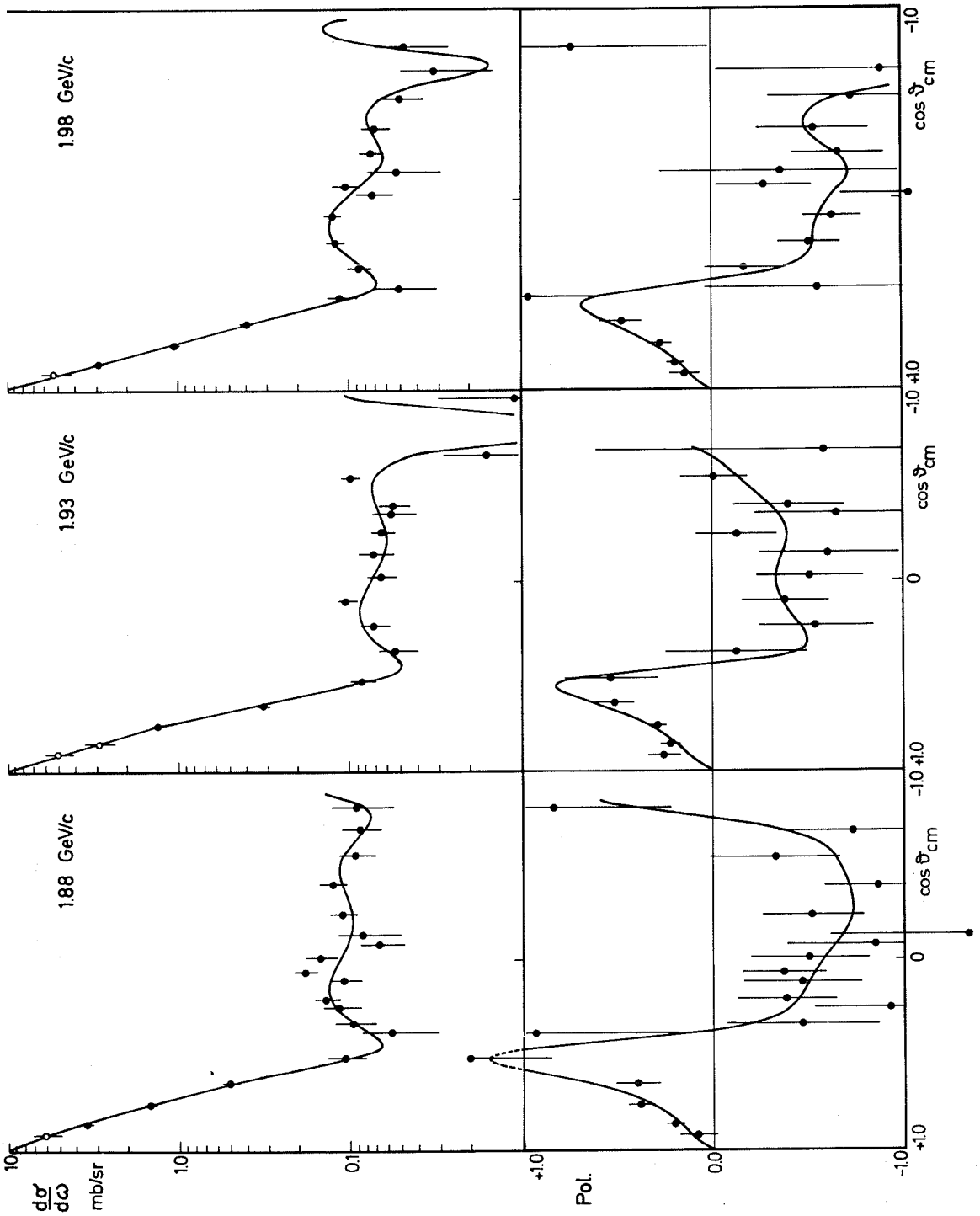
1.98 GeV/c
1.93 GeV/c
1.88 GeV/c
dσ/dω mb/sr
10
1.0
0.1
Pol.
+1.0
0.0
-1.0
cos ϑcm
-1.0
0
+1.0

Fig. 9

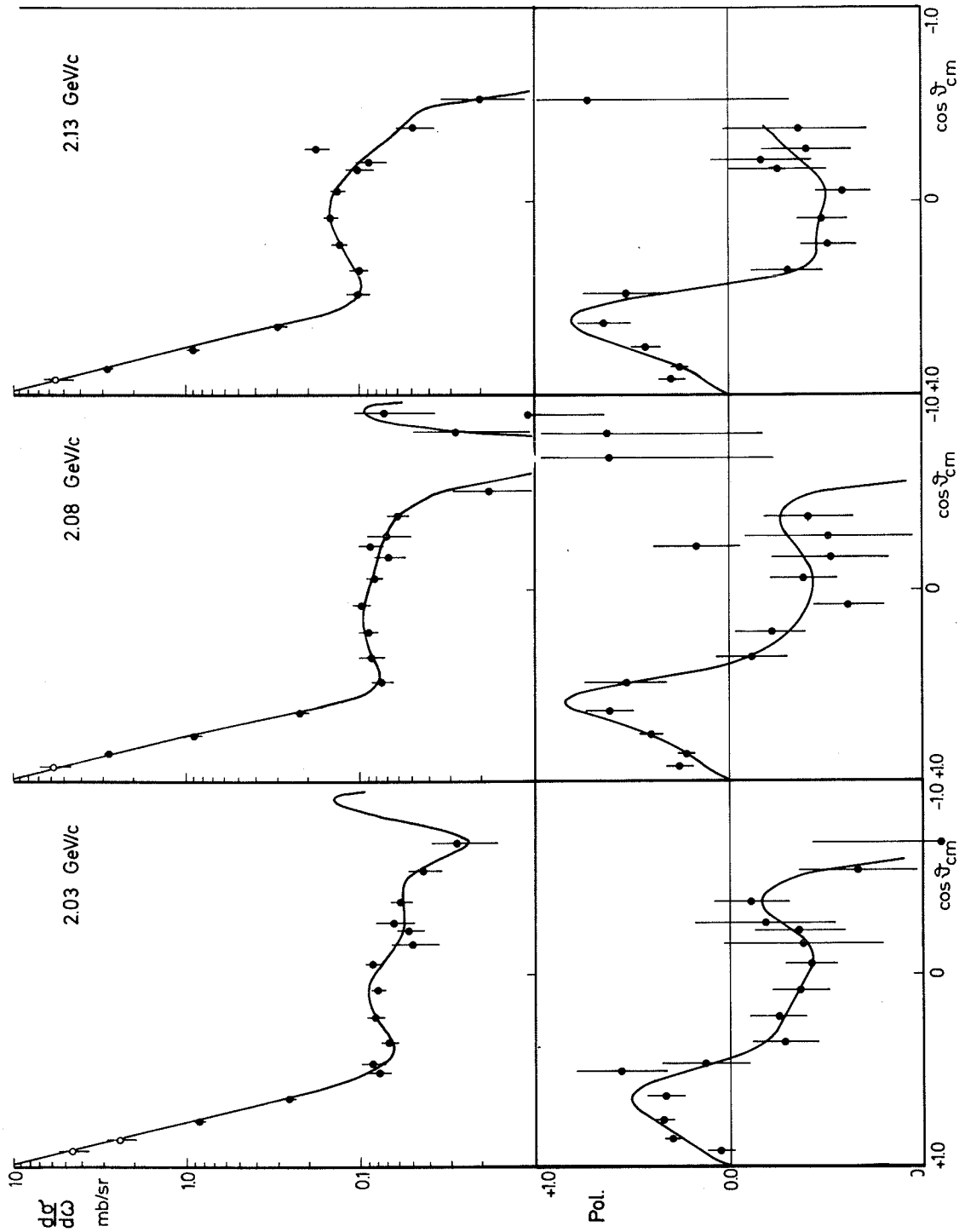
2.13 GeV/c
2.08 GeV/c
2.03 GeV/c
dσ/dΩ mb/sr
10
1.0
0.1
Pol.
+1.0
0.0
-1.0 +1.0
cos ϑcm
-1.0
0
+1.0

Fig. 10

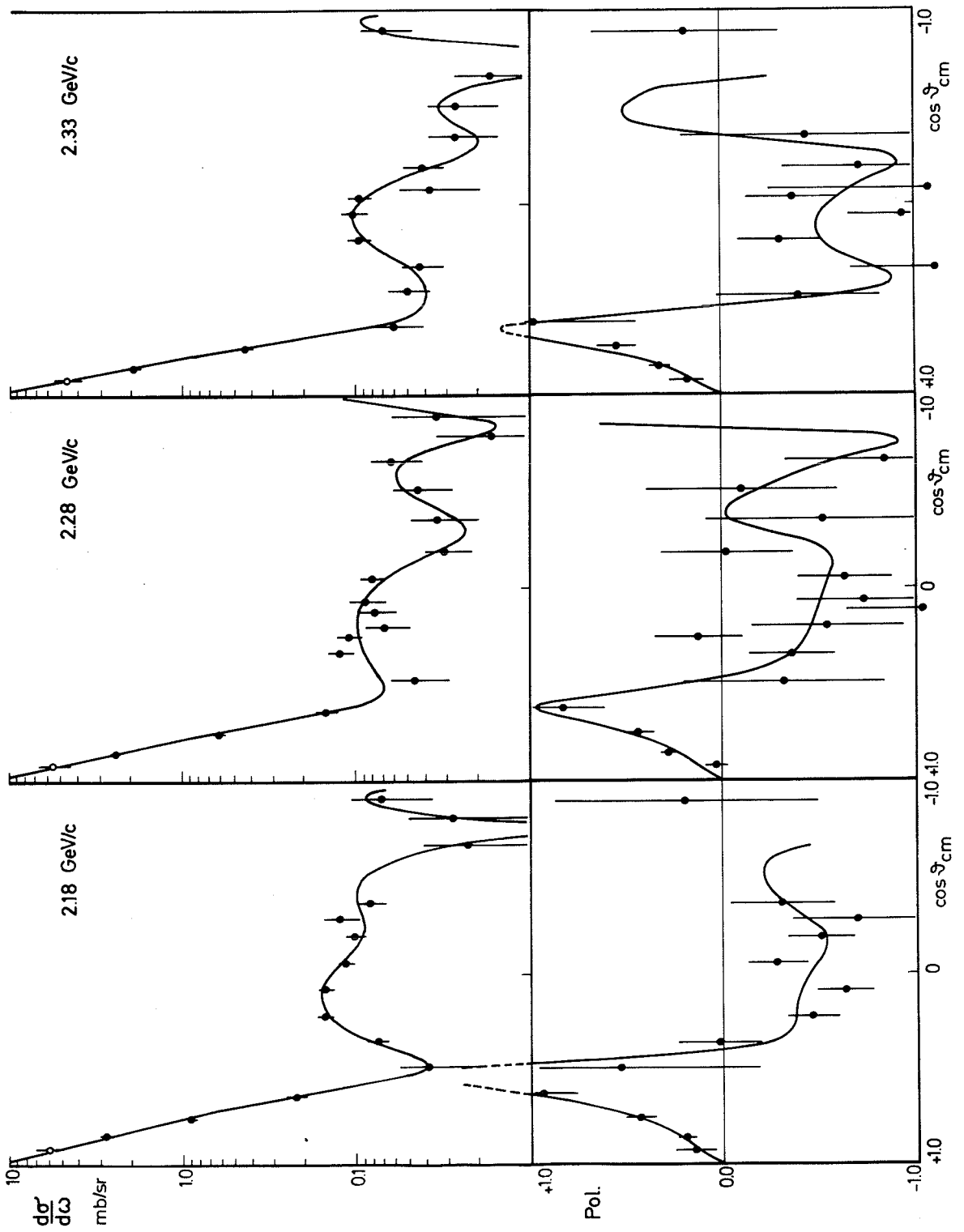
2.33 GeV/c
2.28 GeV/c
2.18 GeV/c
dσ/dω mb/sr
10
1.0
0.1
Pol.
+1.0
0.0
-1.0
cos ϑcm
-1.0
0
+1.0

Fig. 11

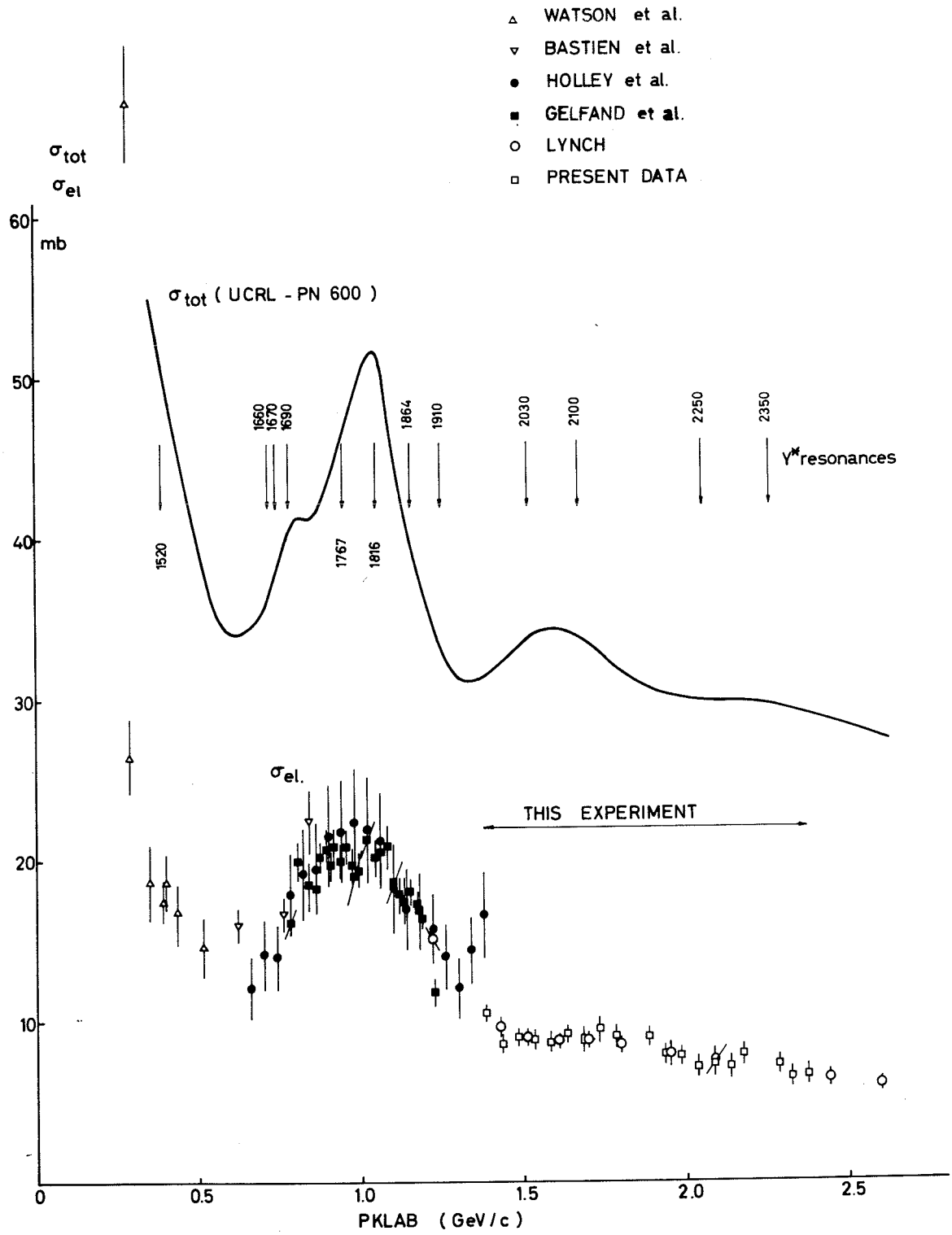
WATSON et al.
BASTIEN et al.
HOLLEY et al.
GELFAND et al.
LYNCH
PRESENT DATA
σtot
σel
60
mb
σtot (UCRL - PN 600)
50
40
30
20
10
1660
1670
1690
1864
1910
2030
2100
2250
2350
Y* resonances
1520
1767
1816
σel.
THIS EXPERIMENT
0
0.5
1.0
1.5
2.0
2.5
PKLAB (GeV/c)

Fig. 12

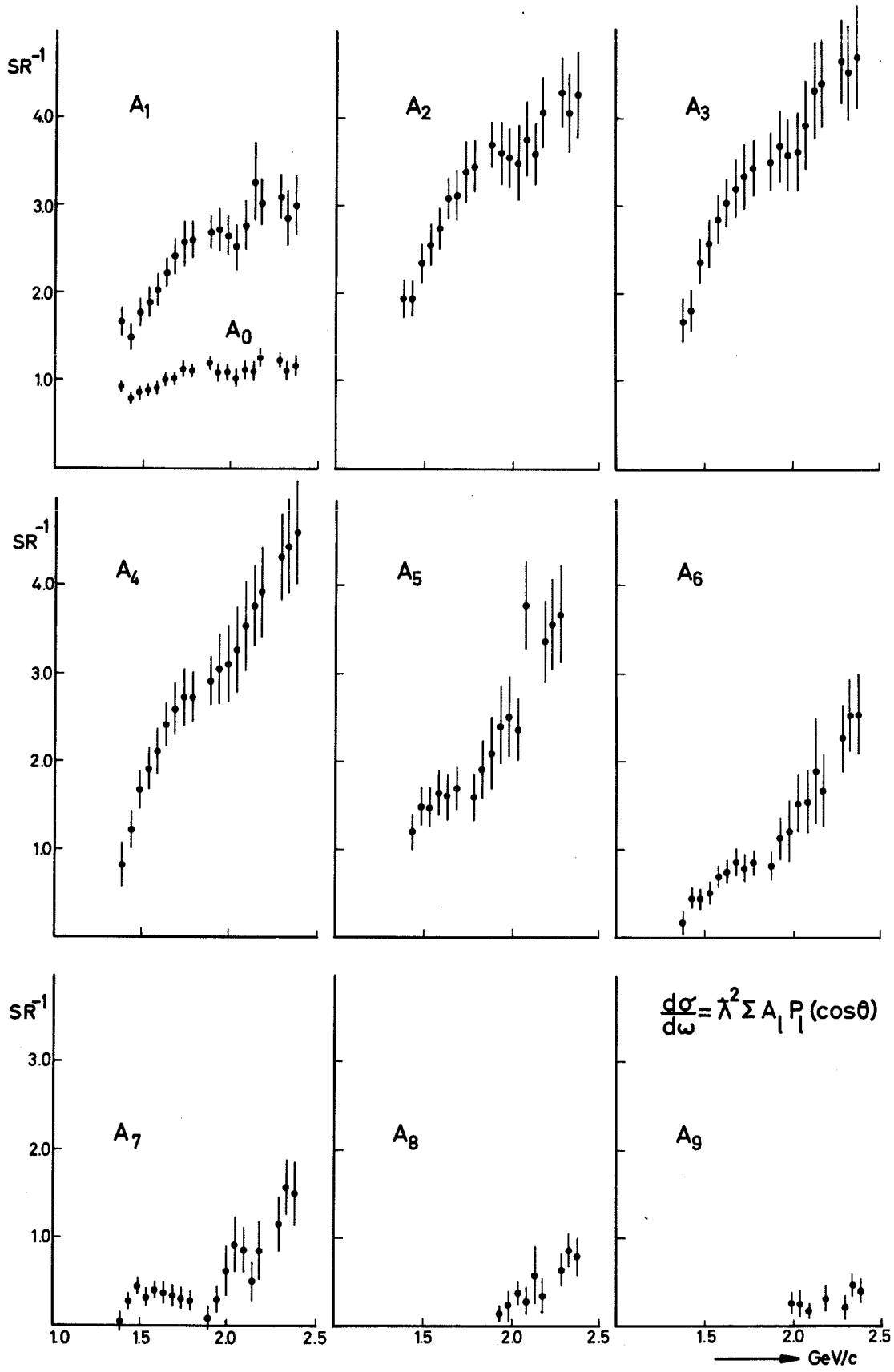

Fig. 13

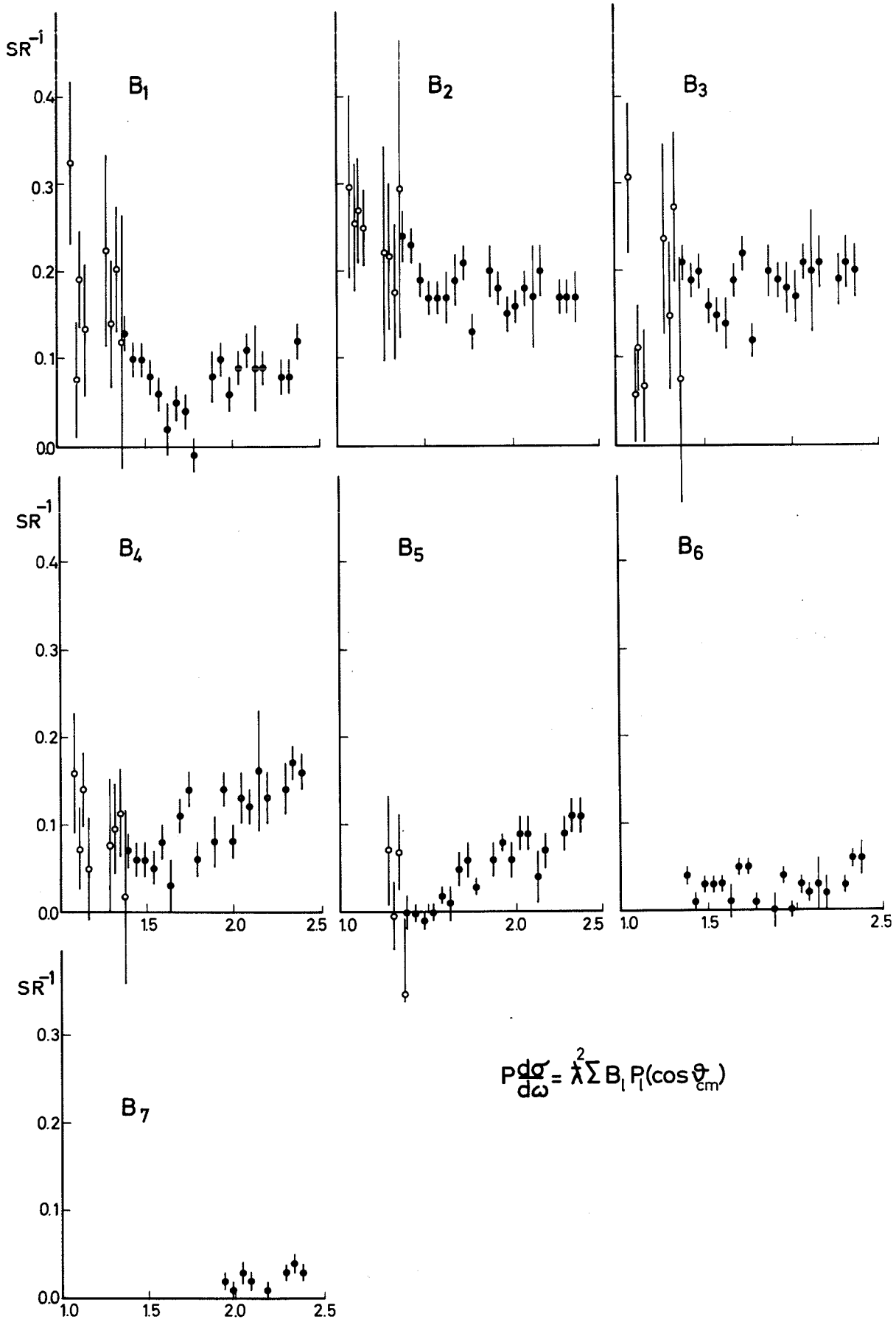

Fig. 14

DIA 33582

POLARIZATION AT $\cos\theta_{cm}=0$

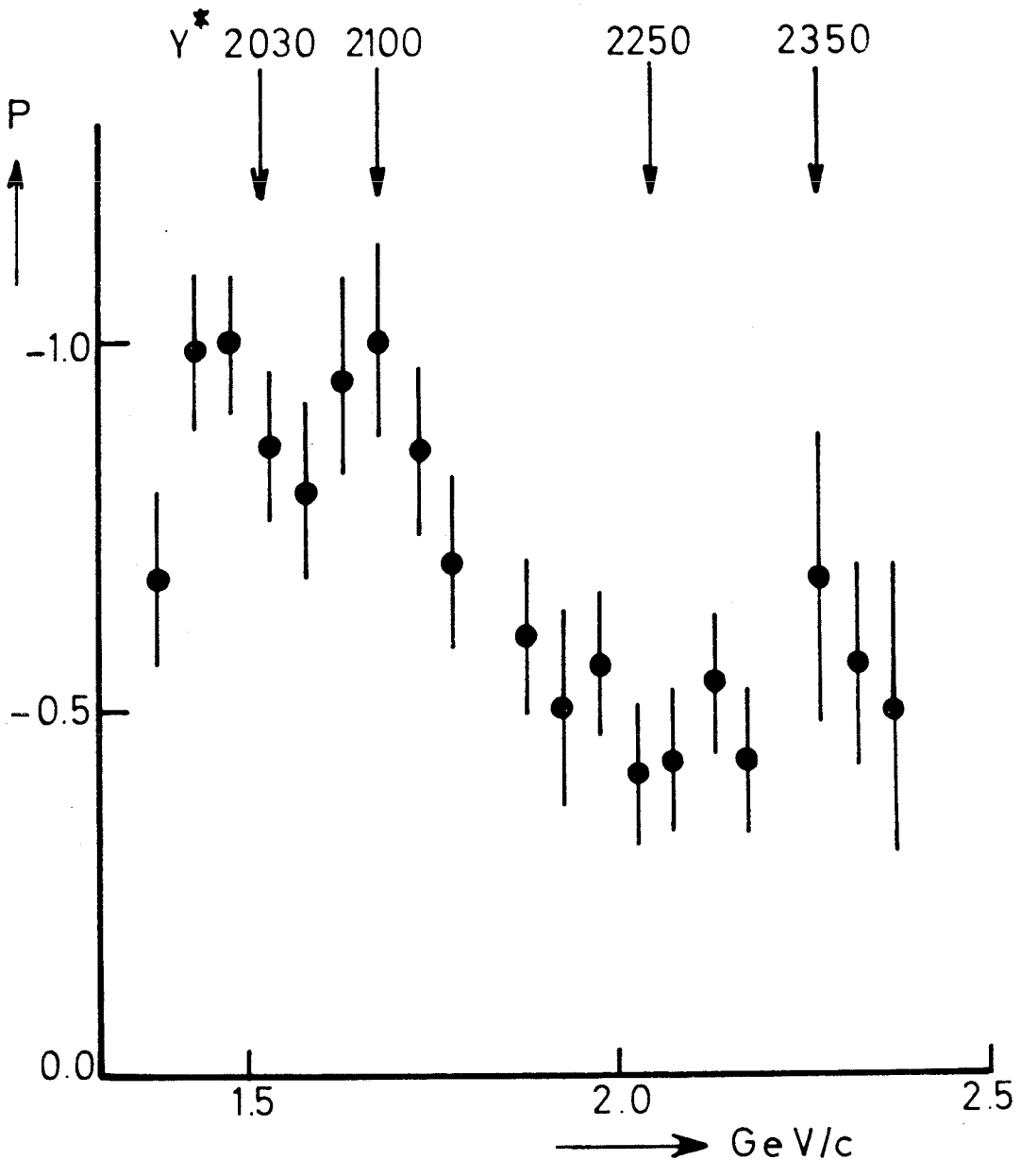

Fig. 15